



Increasing operational stability of journal bearing in hydraulic suspension micro-pump by herringbone grooved structure

Journal:	<i>Science China Technological Sciences</i>
Manuscript ID	SCTS-2023-0024.R3
Manuscript Type:	Original Article
Date Submitted by the Author:	19-May-2023
Complete List of Authors:	Hong, Tao Xing, Guanying Zuo, Huaiyu Xue, Song Luo, Xiaobing
Keywords:	journal bearing, herringbone groove, hydrodynamic effect, micro-pump
Speciality:	Hydraulic Engineering

SCHOLARONE™
Manuscripts

Response Letter

Dear editor and referees,

Please find the revised manuscript of SCTS-2023-0024 which has been resubmitted to *SCIENCE CHINA Technological Sciences*. We are grateful for the referees' valuable comments, which have been carefully addressed in the revised manuscript with the related changes marked in red. A point-by-point reply to the referee's comments is appended below. Thanks for your time and for considering our revised manuscript.

Best regards,

Tao Hong on behalf of co-authors

Response to the reviewer and editor's comments:

Reviewer#1

Comment 1:

The manuscript is improved. Whereas citations of References need further improved, especially the names of authors such as [1] Nisar A A N M B. [16] Xiaobing Luo F L B D. [23] Zhu J O K. [35] Wang Bin S Y T D.

Response:

Thanks for discovering the mistake. We have checked all the references carefully. The correct format of the reference has been modified.

[1] Nisar A, Afzulpurkar N, Mahaisavariya B.

[16/19] Luo X B, Liu F L, Duan B et al.

[23/26] Zhu J, Ono K.

[35/39] Wang Bin, Sun Y T, Ding Q.

Editor

Comment 1:

Please check the journal contents (2021-2023) and consider whether there are more relevant articles that can be referred.

Response:

We have added four references, they are respectively:

[7] Liu P, Ren T, Ge Y et al. Performance Analyses of a Novel Finned Parabolic Trough Receiver with Inner Tube for Solar Cascade Heat Collection. *Sci China Tech Sci*, 2023, 5: 1417-1434

[8] Zhang J, Chen Y, Liu Y et al. Experimental Investigation on Heat Transfer Characteristics of Microcapsule Phase Change Material Suspension in Array Jet Impingement. *Sci China Tech Sci*, 2022, 7: 1634-1645

[14] Wang C, Wang F, An D et al. A General Alternate Loading Technique and its Applications in the Inverse Designs of Centrifugal and Mixed-Flow Pump Impellers. *Sci China Tech Sci*, 2021, 4: 898-

918

[27] Xu J, Jiao C, Zou D et al. Study on the Dynamic Behavior of Herringbone Gear Structure of Marine Propulsion System Powered by Double-Cylinder Turbines. Sci China Tech Sci, 2022, 3: 611-630

Comment 2:

Please upload files: main document.

Response:

We have compressed and uploaded the materials according to the format requirements.

Comment 3:

Please refer to the Template (<http://tech.scichina.com>). The final version will not be allowed to change in content generally.

Response:

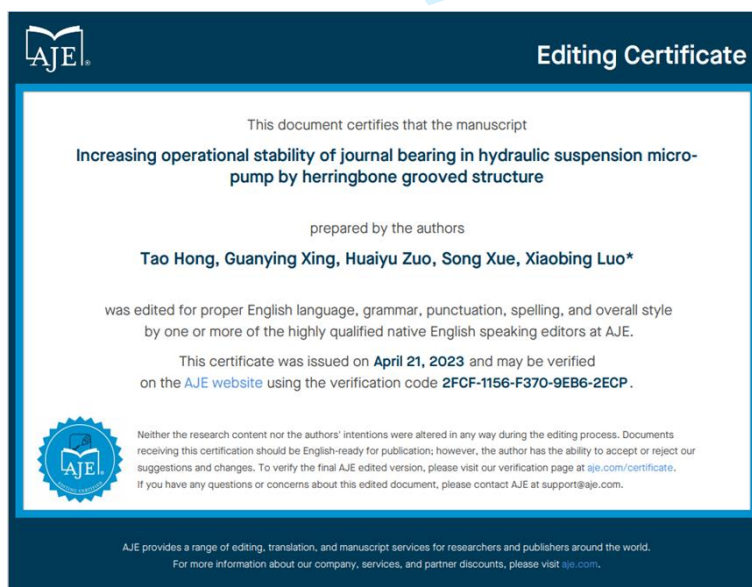
We revised the format of the manuscript based on the template. We checked all references and merged tables with only two rows (table2 and 3).

Comment 4:

We have raised the language requirements. Please check the language carefully. If there are more than three mistakes, we will find the language service companies to polish the language, and the invoice will merge with the page charges. If you have the polish certificate, you can upload it.

Response:

Professional editing services (American Journal Experts) have been used to polish manuscript. The certificate is shown below.

**Comment 5:**

To promote the effect and citation of English articles, a Chinese abstract will be added in the content of our Chinese journal 《中国科学：技术科学》 of the same issue. Please provide the title, authors, abstract, and keywords in Chinese.

Response:

The document of the Chinese abstract is uploaded in the compressed package of the main document.

Comment 6:

Please note in the Cover Letter:

(1) How many single-print with cover and catalogue (30 RMB, at least 10 copies) would like to add for collection and communication (the invoice will merge with the page charges). No free publication to send from 2020.

(2) Please list 5-10 active authors (high cited authors) of this field, including the name and email.

Response:

(1) I'm sorry to tell you that we don't need it

(2) We looked for active authors in the field, and they were:

Ding Qian (qding@tju.edu.cn)

Yin Zhongwei (yinzw@sjtu.edu.cn)

Sunil Kumar (sunil.sharma@chitkara.edu.in)

Nathi Ram Chauhan (nrchauhan@igdtuw.ac.in)

Pankaj khatak (pankajkhatak@gmail.com)

Increasing operational stability of journal bearing in hydraulic suspension micro-pump by herringbone grooved structure

Tao Hong, Guanying Xing, Huaiyu Zuo, Song Xue, Xiaobing Luo*

State Key Laboratory of Coal Combustion, School of Energy and Power Engineering

Huazhong University of Science and Technology, Wuhan 430074, China

*luoxb@hust.edu.cn

Abstract

The operational stability of radial journal bearings is the bottleneck that limits the reliability of hydraulic suspension micro-pump. Due to self-excited vibrations, the whirl amplitude of the plain journal bearing (PJB) is large at high rotational speeds, which will accelerate wear failure. It has been proven that employing herringbone grooved journal bearing (HGJB) is an effective method to reduce the whirl amplitude and improve operational stability. However, enhancing the stability of journal bearings in micro-pumps by herringbone grooved structures has rarely been studied, and its effect needs to be verified. We validated the mechanism of the stability improvement with the CFD method and compared the dynamic characteristics of HGJB and PJB by rotor dynamics evaluation and experiment. The experimental results show that under the same conditions the whirl amplitude of the HGJB decreases by 29.61% in the X direction and by 24.09% in the Y direction compared with that of the PJB. This study reveals the effect of the herringbone grooved structure on the operational stability of bearings and may provide guidance for the reliability improvement of hydraulic suspension micro-pump.

Key words: journal bearing; herringbone groove; hydrodynamic effect; micro-pump.

1. Introduction

A micro-pump is the power source of microfluidic delivery, which is widely used in the fields of drug delivery [1, 2], artificial hearts [3, 4], electronic cooling systems [5-8], etc., and has broad application prospects [9]. According to the difference in working principles, micro-pumps can be divided into piezoelectric pumps [10], electroosmotic pumps [11], electrohydrodynamic pumps [12], and centrifugal pumps [13, 14]. Among them, centrifugal pumps have the advantages of high hydraulic performance and good adjustability, thus, they have become a promising choice for driving microfluidic systems. Centrifugal pumps can be divided into contact bearing pumps and suspension bearing pumps according to the supporting mode of the rotor [15, 16]. The problem of the contact bearing pump is mechanical friction, which restricts the reliability and endurance in application [16, 17]. To prevent contact wear problems, we developed a kind of hydraulic suspension micro-pump with a radial journal bearing in our previous works [18, 19]. The hydrodynamic effect makes the rotating components levitate, which prevents contact with other components, thus greatly improving the theoretical life of the micro-pump.

The radial suspension bearing used in this micro-pump is essentially a plain journal bearing (PJB), which is widely used in rotating machines. The journal is set eccentrically relative to the bearing, and the liquid film in the convergence zone produces a dynamic pressure effect when the journal rotates. This pressure balances the load on the journal and separates the journal from the inner wall of the bearing. However, the supporting force produced by the liquid film is not collinear with the eccentric direction of the journal, causing a moment that will promote the whirl of the journal. The moment will generate self-excited vibrations at high speeds, and the journal will no longer be in a steady state. As a result, when the whirl amplitude increases, collisions between the journal and bearing may occur,

1
2
3 seriously affecting the performance and reliability of the pump. At present, researchers have carried out
4 a series of studies on increasing PJB operational stability. Kumar and Garg et al. found that the
5 viscosity of the lubricant has a significant influence on the dynamic characteristics of a PJB, and the
6 use of magnetic fluids or certain non-Newtonian fluids can improve the operational stability of a PJB
7 [20, 21]. However, the fluid choice depends on the function of the microfluidic system, making the
8 viscosity change impractical. Alternatively, adding external support, such as that used in floating ring
9 bearings, provides an effective means for increasing operational stability. The bearing is installed on
10 the external film with appropriate damping, which can absorb vibration energy and greatly reduce the
11 whirl amplitude of the bearing [22]. However, external support will inevitably reduce the power density
12 and increase the complexity of the system. In addition, reducing the bearing width has also been proven
13 to be an effective method to improve operational stability [23]. Nonetheless, simply reducing the width
14 will increase the end leakage and decay the loading performance of the journal bearing. In addition, the
15 motor design determines the width of the rotor, thus limiting the structure optimization of the journal
16 suspension. In summary, the three methods mentioned above are not applicable in hydraulic suspension
17 micro-pump. In recent years, the method of machining microgrooves on the journal surface has become
18 an effective means to improve the stability of journal bearings due to its advantages of reliability and
19 efficiency, which can improve operational stability by strengthening the local hydrodynamic effect [24].
20 To date, grooved bearings have been widely used in bearings with gas, liquid, and grease as lubricants,
21 especially in miniaturized bearings [25-27].

22
23 Among the various shapes of grooves, the herringbone groove, which can suppress whirl
24 instability, has aroused widespread attention. The mechanism can be explained as follows: when the
25 journal rotates, the groove restricts the flow of fluids, which causes the fluids to converge at the cusp,
26 forming a pumping effect [24], thus enhancing the local pressure and improving the dynamic
27 characteristics of the journal bearing. Narrow groove theory (NGT) has been proposed to investigate
28 the suspension characteristics of a herringbone grooved journal bearing (HGJB) [28, 29], which assumes
29 that the number of grooves is infinite, while for an HGJB with finite slots, its accuracy is unsatisfying.
30 Alternatively, the finite difference method (FDM) [30-32] and finite element method (FEM) [33, 34] are
31 used to solve the nonlinear Reynolds equation numerically and are sufficiently accurate compared to
32 the experiments. Furthermore, Hirs [35] and Gao [36] experimentally studied a hydrodynamic HGJB and
33 an aerostatic HGJB and obtained better stability compared to a PJB. In addition, an HGJB can
34 significantly restrain the radial runout of the high-speed spindle and increase the maximum operating
35 speed [37]. Due to its excellent dynamic properties, HGJBs have been used in high-speed light-load
36 rotating machinery, such as high-precision machine tool spindles and hard disks. Moreover, there are
37 few studies that use herringbone grooves to improve the stability of radial suspension bearings in
38 micro-pump. Inspired by this, we employ an HGJB to improve the operational stability of the
39 micro-pump, conduct theoretical modeling and analysis to explore its dynamic and static characteristics,
40 and verify its effect by experiments.

41
42 In this work, we developed a herringbone grooved structure on a journal bearing applied in a
43 micro-pump. The comprehensive effect of herringbone grooves on water-lubricated journal bearings is
44 studied numerically and experimentally. By CFD simulation, the pressure distribution and bearing
45 capacity of the HGJB and PJB at different eccentricities are studied comparatively. Moreover, based on
46 the perturbation method, the stiffness and damping coefficients are solved to clarify the rotor dynamic
47 characteristics. Then, the critical mass is obtained by solving the rigid body motion equation, and the
48 stability of the HGJB and PJB is evaluated. Finally, the veracity of the theoretical analysis is verified
49
50
51
52
53
54
55
56
57
58
59
60

by experiments.

2. Operating Principle of the Hydraulic Suspension Micro-pump with the PJB and the HGJB

Fig. 1 shows the structure of the hydraulic suspension micro-pump with the radial suspension bearing proposed in our previous work [18, 19, 38]. The journal bearing is composed of a rotor inside a sleeve, with a small clearance between them for fluid flow. Due to the eccentric placement of the journal, when the journal rotates, the thickness of the liquid film changes along the direction of rotation, forming a convergent region (part I in Fig. 1) on the right side of line OO_1 and a diverging region (part II in Fig. 1) on the left side. Due to the hydrodynamic effect, the liquid film of the convergent region generates high pressure, and the pressure of the diverging region decreases rapidly, thus constructing the pressure difference between the two regions and providing the radial suspension force.

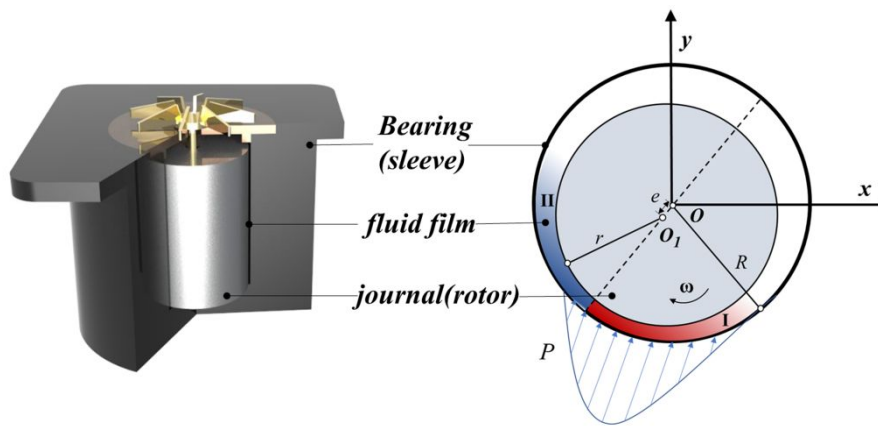


Fig. 1 Schematic diagram of the journal bearing in the hydraulic suspension micro-pump

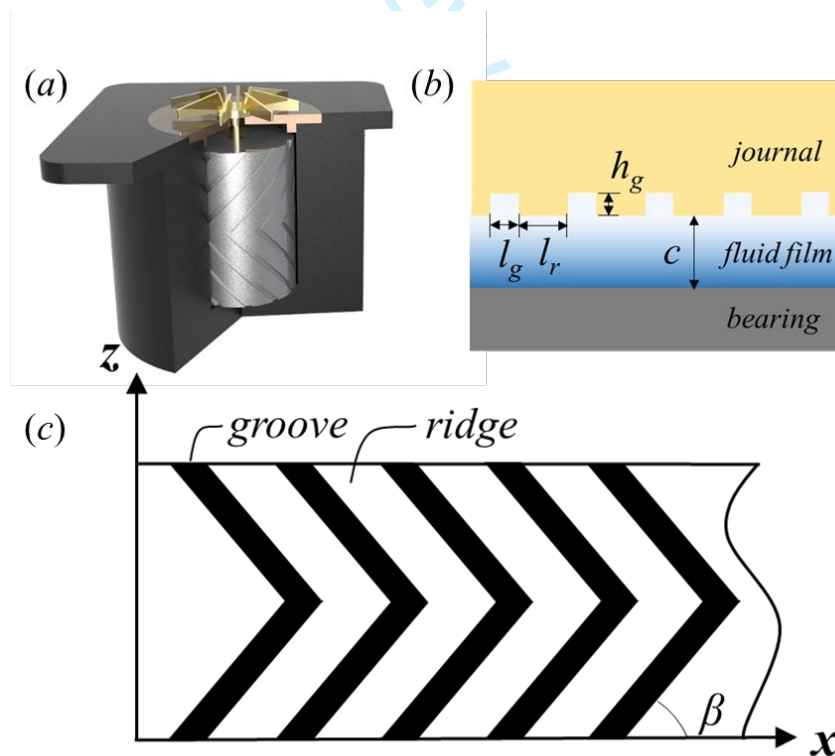


Fig. 2 (a) 3D rendered graph of the HGJB in a micro-pump. (b) cross-sectional view of the HGJB. (c) Radial expansion diagram of the herringbone grooved structure.

The HGJB employed in this paper has a rectangular section, and the structure of the HGJB is shown in Fig. 2. The main structural parameters are shown in Table 1, where the groove number $n=12$, helix angle $\beta=45^\circ$, groove width $l_g=0.6$ mm and groove depth $h_g=28.5$ μm . It should be mentioned that the values of the groove number and helix angle are referred to Bin Wang's work [39], and the depth and width of the groove are determined by the machining precision. Thus, we believe that the working performance of the HGJB may be better if the geometrical parameters are optimized further.

Table 1 Structure parameters of the PJB and HGJB.

Type	length l (mm)	radius r (mm)	clearance c (mm)	n	β ($^\circ$)	l_g (mm)	h_g (μm)
PJB	17.2	6.33	0.07	/	/	/	/
HGJB	17.2	6.33	0.07	12	45	0.6	28.5

3. Methods

3.1 Experimental Setup

Distinctly, the stability of journal bearings can be reflected by the journal's whirl tail. To observe it accurately, a test facility is constructed, and Fig. 3 (a) shows the overall schematic diagram of the test facility. To measure the real-time position of the journal, two laser displacement sensors (Keyence, LK-H020) with ± 1 μm accuracy are installed on two micro-displacement stages (LD60-LM-2). The HGJB is assembled into a micro-pump with acrylic volute, whose transmissivity is high (more than 90%), allowing the laser to flash on the bearing. The inlet and outlet tubes of the micro-pump are connected to a water sink. To reduce the interference of external vibrations and ensure sufficient levelness, the working micro-pump is installed on a specific fixture, and the entire test facility is installed on a high-precision optical platform.

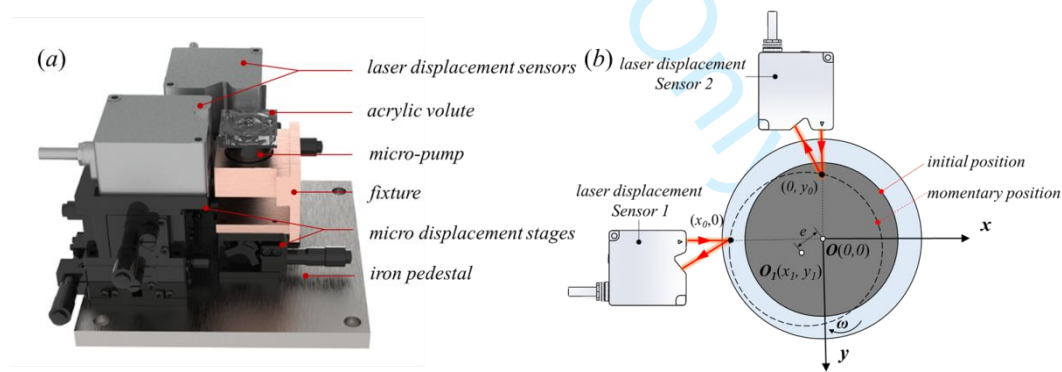


Fig. 3 (a) Overall schematic diagram of the test facility. (b) Schematic diagram of the experimental test principle.

The test principle in this work is shown in Fig. 3 (b). Two laser displacement sensors are arranged vertically in the radial direction of the micro-pump. The laser flashes on the journal through the acrylic volute, and then the reflected light returns to the receiver. The data x_0 and y_0 are directly recorded by laser displacement sensors. The momentary position (x_1, y_1) of the rotor can be calculated by combining Eq. (1) and (2), and the eccentricity e is denoted below.

$$(x_0 - x_1)^2 + (0 - y_1)^2 = r^2 \quad (1)$$

$$(0 - x_1)^2 + (y_0 - y_1)^2 = r^2 \quad (2)$$

$$e = \sqrt{x_1^2 + x_2^2} \quad (3)$$

3.2 Numerical Simulation

Numerical simulations are conducted to investigate the dynamic coefficients and pressure distributions of the HGJB and the PJB by using COMSOL MULTIPHYSICS 5.6. Fig. 4 shows the journal film domains of the PJB and the HGJB used in the simulation. Structured meshes are used for the PJB, and unstructured meshes are used for the HGJB. As shown in Fig. 4, to capture the fluid flow process and pressure distribution details, grids are meshed finer in the herringbone groove zone. The pressure boundary condition of the inlet and outlet is set to zero pressure. The flow state of the liquid is judged by the critical Reynolds number formula of the concentric cylinder in Eq. (4) [40]. The Reynolds numbers of the PJB and HGJB are calculated as follows.

$$Re_c = 41.1 \sqrt{\frac{R}{C}} \quad (4)$$

$$Re = \frac{\rho u d}{\mu} \quad (5)$$

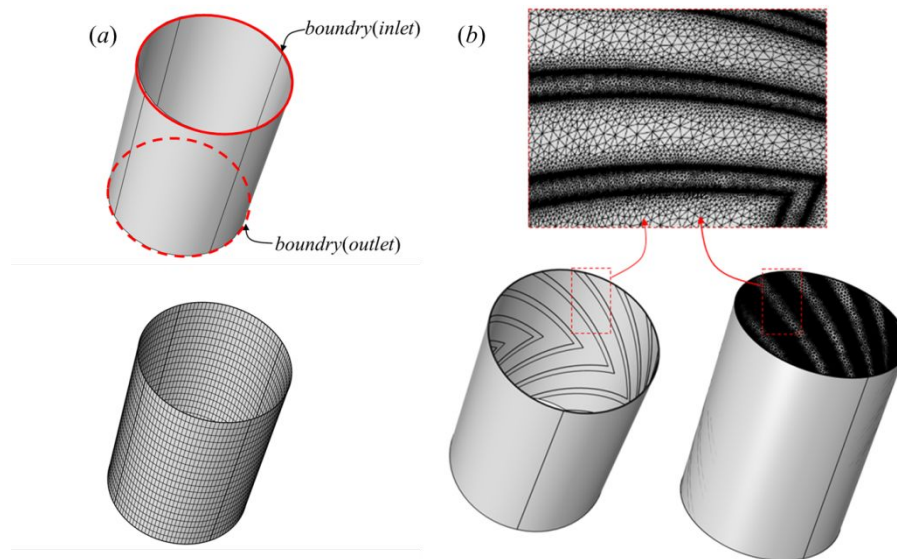


Fig. 4 Simulation models of the PJB (a) and the HGJB (b).

In this simulation, 20°C water is used as lubricant, and the density and dynamic viscosity are set to 998.2 kg/m³ and 1.006 mPa·s, respectively. The grid independence tests are performed at a rotating speed of 15000 RPM and eccentricity of 0.1. The maximum pressures of the HGJB are calculated with grid numbers of 41836, 132184, 443867, and 737229. The results are shown in Table 2. Similarly, the grid independence results of the PJB are shown in Table 2 too. Taking computation cost into consideration, the mesh scheme with a grid number of 443867 is used for the HGJB, while a grid number of 2400 is used for the PJB.

Table 2 Grid independence verification results of the HGJB and PJB.

HGJB	Grid number	41836	132184	443867	737229
	Max pressure	6066.5	6069.8	6074.9	6077.1
PJB	Grid number	2400	3200	4800	6400
	Max pressure	3170.6	3170.6	3170.6	3170.6

3.3 Numerical Method Verification

Based on the numerical simulation method mentioned earlier, the performance of journal bearings is studied. To validate this method, six cases are studied, and the numerical results are compared with the experimental data of Gao and Yin's work [41].

Gao and Yin's experiment used 20°C water as lubricant to test the eccentricity of bearings under six working conditions, as listed in Table 3, including different rotating speeds and loads. Fig. 5 is a comparison of the numerical calculation results and Gao and Yin's experimental data under six working conditions. The results show that the numerical calculation results match well with the experimental data, and the maximum error is less than 8.45%.

Table 3 Working conditions of Gao and Yin's experiment.

Case	Rotating speed	Load
1	1500 RPM	2050 N
2	2000 RPM	2700 N
3	2500 RPM	3350 N
4	3000 RPM	3950 N
5	3500 RPM	4850 N
6	4000 RPM	5200 N

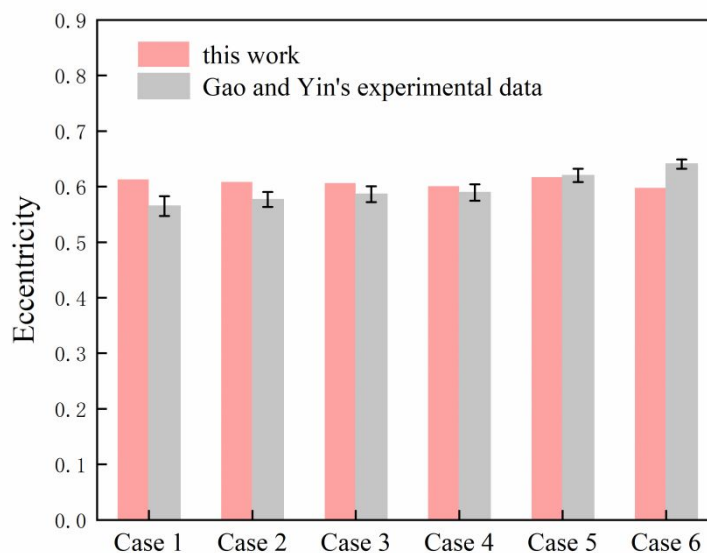


Fig. 5 Simulation model of the PJB (a) and the HGJB (b).

3.4 Rotor Dynamic Calculation

From the viewpoint of rotor dynamics, the liquid film usually acts as a nonlinear spring and damper, which has a great influence on the dynamic characteristics of the whole system. In the study of journal bearings, because most of them involve only small or infinitesimal amplitudes, the stiffness coefficient and damping characteristics of the liquid film are considered to be linear.

Assuming that the journal is in static equilibrium, a Taylor expansion is carried out for the bearing capacity in the x and y directions. After ignoring higher-order terms, the bearing capacity is given as follows:

$$\begin{aligned} F_x &= F_{x0} + \left(\frac{\partial F_x}{\partial x} \right)_0 \Delta x + \left(\frac{\partial F_x}{\partial y} \right)_0 x \Delta y + \left(\frac{\partial F_x}{\partial x'} \right)_0 x' + \left(\frac{\partial F_x}{\partial y'} \right)_0 xy' \\ F_y &= F_{y0} + \left(\frac{\partial F_y}{\partial x} \right)_0 \Delta x + \left(\frac{\partial F_y}{\partial y} \right)_0 x \Delta y + \left(\frac{\partial F_y}{\partial x'} \right)_0 x' + \left(\frac{\partial F_y}{\partial y'} \right)_0 xy' \end{aligned} \quad (6)$$

It can be seen that the coefficient of the original term in Eq. (6) has a stiffness dimension, and the coefficient of the first-order term has a damping dimension. After simplification, it can be expressed by Eq. (7)

$$\begin{pmatrix} \Delta F_x \\ \Delta F_y \end{pmatrix} = \begin{pmatrix} K_{xx} & K_{xy} \\ K_{yx} & K_{yy} \end{pmatrix} \begin{pmatrix} \Delta x \\ \Delta y \end{pmatrix} + \begin{pmatrix} C_{xx} & C_{xy} \\ C_{yx} & C_{yy} \end{pmatrix} \begin{pmatrix} x' \\ y' \end{pmatrix} \quad (7)$$

where K_{xx} and K_{yy} are direct stiffness coefficients, K_{xy} and K_{yx} are cross stiffness coefficients, C_{xx} and C_{yy} are direct damping coefficients, C_{xy} and C_{yx} are cross damping coefficients, Δx and Δy are displacements, and x' and y' are the velocities. The dynamic characteristics of the HGJB and the PJB are calculated by the pressure perturbation method^[42]. The calculation method is denoted as follows:

$$K_{xx} = \frac{\Delta F_{sxx}}{\Delta x} \quad K_{xy} = \frac{\Delta F_{sxy}}{\Delta y} \quad K_{yx} = \frac{\Delta F_{syx}}{\Delta x} \quad K_{yy} = \frac{\Delta F_{syy}}{\Delta y} \quad (8)$$

$$C_{xx} = \frac{\Delta F_{vxx}}{x'} \quad C_{xy} = \frac{\Delta F_{vxy}}{y'} \quad C_{yx} = \frac{\Delta F_{vyx}}{x'} \quad C_{yy} = \frac{\Delta F_{vyy}}{y'} \quad (9)$$

In Eq. (8), ΔF_{sij} is the variation in fluid film capacity caused by displacement perturbation, $\Delta F_{sij} = F_{sij} - F'_{sij}$, where F_{sij} is the liquid film capacity in the equilibrium state, and F'_{sij} is the liquid film capacity after the displacement perturbation is applied. In Eq. (9), ΔF_{vij} is the variation in the fluid film capacity caused by the velocity perturbation. $\Delta F_{vij} = F_{vij} - F'_{vij}$, where F_{vij} is the liquid film capacity in the equilibrium state, and F'_{vij} is the liquid film capacity after the velocity perturbation is applied.

The dynamic characteristic parameters of liquid films are very important for studying the stability of journal bearings. Generally, the larger the stiffness of the liquid film is, the stronger the bearing capacity, and the larger the damping is, the better the stability. Furthermore, the influence of stiffness and damping need to be considered simultaneously when studying the stability of a journal bearing, and the optimization approach must be based on the coupling effect between them to achieve the best stability. The system stability is characterized by the critical journal mass, which is determined by the stiffness coefficient, damping coefficient and journal mass. By substituting Eq. (6) into instantaneous dynamic Eq. (10),

$$\begin{aligned} mx'' + \Delta F_x &= 0 \\ my'' + \Delta F_y &= 0 \end{aligned} \quad (10)$$

The dynamical equation of journal bearings can be expressed as Eq. (11):

$$\begin{aligned} mx'' + K_{xx}\Delta x + K_{xy}\Delta y + C_{xx}x' + C_{xy}y' &= 0 \\ my'' + K_{yx}\Delta x + K_{yy}\Delta y + C_{yx}x' + C_{yy}y' &= 0 \end{aligned} \quad (11)$$

Eq. (11) is a linear equation whose general solution is shown below, where ν is the eigenvalue and is a complex number.

$$\begin{aligned} \Delta x &= x_0 e^{\nu t} \\ \Delta y &= y_0 e^{\nu t} \end{aligned}$$

(12)

By substituting Eq. (12) into Eq. (11), the characteristic equation is given as :

$$\begin{aligned} (m\nu^2 + C_{xx}\nu + K_{xx})x_0 + (C_{xy}\nu + K_{xy})y_0 &= 0 \\ (C_{yx}\nu + K_{yx})x_0 + (m\nu^2 + C_{yy}\nu + K_{yy})y_0 &= 0 \end{aligned}$$

(13)

In the critical state, there exists an eigenvalue ν that is a pure imaginary number. Here, $\nu = i\omega_{st}$, and ν is substituted into Eq. (10); it can be expressed as:

$$\begin{aligned} \Delta F_x &= m\omega_{st}^2 x_0 e^{i\omega_{st}t} = m\omega_{st}^2 \Delta x \\ \Delta F_y &= m\omega_{st}^2 y_0 e^{i\omega_{st}t} = m\omega_{st}^2 \Delta y \end{aligned} \quad (14)$$

where ω_{st} is the critical whirl frequency. In the critical state, the proportional coefficient between ΔF_x and Δx , ΔF_y and Δy is $m\omega_{st}^2$. This indicates that the liquid film at this time is equivalent to an isotropic spring with similar dynamic characteristics, and its stiffness is called the equivalent stiffness, which is expressed by K_{eq} as follows:

$$K_{eq} = m\omega_{st}^2 \quad (15)$$

By substituting Eq. (15) and $\nu = i\omega_{st}$ into Eq. (13), we obtain:

$$\begin{aligned} (i\omega_{st}C_{xx} + K_{xx} - K_{eq})x_0 + (i\omega_{st}C_{xy} + K_{xy})y_0 &= 0 \\ (i\omega_{st}C_{yx} + K_{yx})x_0 + (i\omega_{st}C_{yy} + K_{yy} - K_{eq})y_0 &= 0 \end{aligned} \quad (16)$$

For Eq. (16), only when a nontrivial solution exists will the determinant of the coefficients equal 0. Then, the motion of the rotor converges. The convergence criterion of the rotor can be expressed as follows:

$$\begin{vmatrix} i\omega_{st}C_{xx} + K_{xx} - K_{eq} & i\omega_{st}C_{xy} + K_{xy} \\ i\omega_{st}C_{yx} + K_{yx} & i\omega_{st}C_{yy} + K_{yy} - K_{eq} \end{vmatrix} = 0 \quad (17)$$

where the equivalent stiffness K_{eq} and the critical whirl frequency ω_{st} can be obtained by expanding the determinant:

$$K_{eq} = \frac{K_{xx}C_{yy} + K_{yy}C_{xx} - K_{xy}C_{yx} - K_{yx}C_{xy}}{C_{xx} + C_{yy}} \quad (18)$$

$$\omega_{st}^2 = \frac{(K_{eq} - K_{xx})(K_{eq} - K_{yy}) - K_{xy}K_{yx}}{C_{xx}C_{yy} - C_{xy}C_{yx}}$$

where K_{eq} reflects the comprehensive stiffness of the liquid film and ω_{st} reflects the development degree of whirl in the liquid film. When the other conditions are consistent, if K_{eq} is larger and ω_{st} is smaller, the stability of the rotor-bearing system is better. Obviously, the equivalent stiffness coefficient of the liquid film should always be greater than zero, and $K_{eq} > 0$ is a necessary condition for system stability. When $\omega_{st} < 0$, even if a perturbation is applied, the whirl will decay quickly; hence, $\omega_{st} < 0$ is the sufficient condition for system stability. Only when $K_{eq} > 0$ and $\omega_{st} > 0$ does the system seem to be unstable. As follows, the ratio of K_{eq} to ω_{st}^2 is the critical journal mass, which is the key indicator for system stability.

$$m_c = \frac{K_{eq}}{\omega_{st}^2} \quad (19)$$

If the actual mass of the rotor is greater than m_c , the rotor motion is divergent, and the system is unstable. In contrast, the rotor motion is convergent, and the system is stable. Furthermore, the larger m_c is, the higher the stability margin of the system is.

4. Results and Discussion

Simulations are carried out at 15000 RPM, which is the typical working speed of this micro-pump. The pressure distribution, bearing capacity and dynamic coefficients of the HGJB and PJB when the eccentricity is 0.1-0.9 are investigated by numerical simulations. Taking the eccentricity of 0.1 as an example, the pressure distribution of the HGJB and PJB are shown in Fig. 6 (a). It can be observed that the hydrodynamic effect of fluid causes a positive-pressure region and a negative-pressure region on the journal surface. It is evident that HGJB produces a higher pressure at the cusp of the herringbone groove than the same position of the PJB. Fig. 6 (b) shows the pressure distribution of the intermediate plane on the HGJB and PJB. The maximum and minimum pressures of the PJB are 3170.7 Pa and -3170.7 Pa, which are symmetrically distributed in the convergent region and diverging region, respectively. The maximum pressure of the HGJB is 8096 Pa, and the minimum pressure is -1784 Pa. There are twelve pressure peaks on the HGJB, which correspond to twelve herringbone grooves on the journal surface. The reason for this phenomenon is that the herringbone grooves restrict the fluid flow in the bearing clearance, and the fluid converges at the cusps, making the local pressure higher than

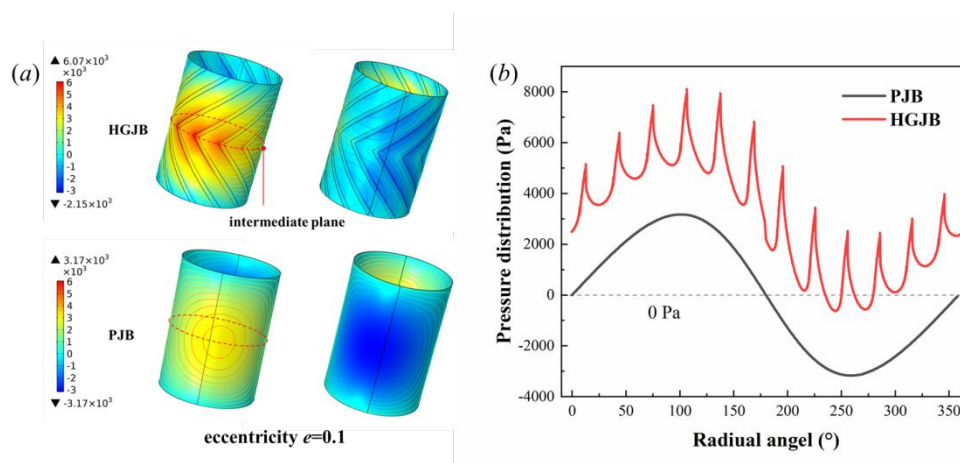


Fig. 6 (a) Pressure distribution contours of the HGJB and PJB.

(b) Pressure distribution on the intermediate circle of the HGJB and PJB varies with radial angle.

As shown in Fig. 7, with increasing eccentricity, the bearing capacity and maximum pressure of the HGJB and PJB increase sharply, while the minimum pressure decreases sharply. When the eccentricity increases, the minimum thickness of the liquid film decreases, and the gradient of the liquid film thickness in the bearing clearance increases, which enhances the hydrodynamic effect of the fluid. As a result, the pressure in the convergent region is higher, the pressure in the diverging region is lower, and the loading capacity is larger. The results show that when the eccentricity is less than 0.55, the minimum pressure of the HGJB is greater than that of the PJB, and the maximum pressure of the HGJB is always greater than that of the PJB. This indicates that the fluid pumping effect brought by the herringbone grooves enhance the positive pressure. Moreover, the force of the convergent region is enhanced while that of the diverging region is weakened. When the eccentricity is less than 0.74, the load capacity of the HGJB is greater than that of the PJB, and it is smaller than that of the PJB when the eccentricity is larger than 0.74. The reason for this phenomenon is that when the eccentricity is at the critical value of 0.74, the strengthening of the force in the convergent region will offset the weakening of the force in the diverging region, making the bearing capacity of the HGJB equal to PJB.

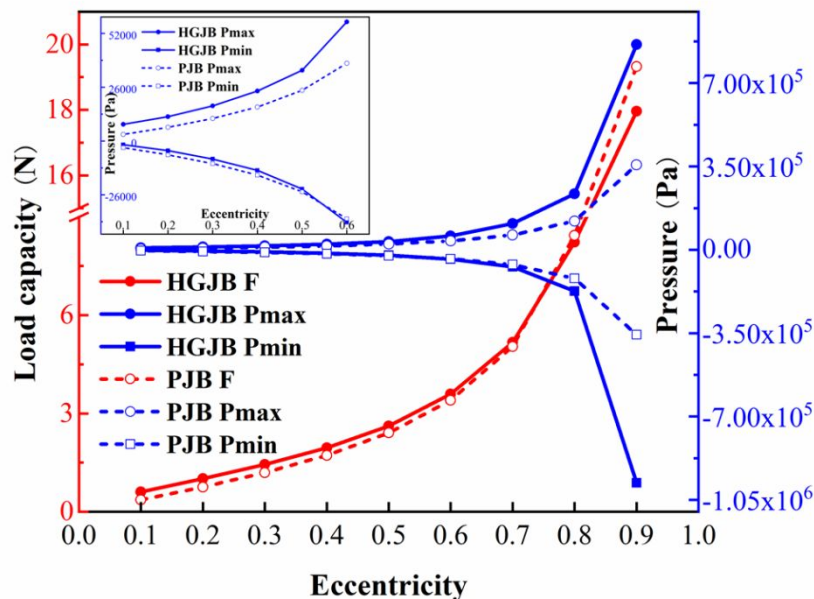


Fig. 7 Journal bearing capacity and the maximum/ minimum pressure of the HGJB and PJB vary with eccentricity.

Fig. 8 shows the variation in the stiffness coefficients and damping coefficients as the eccentricity varies. The results show that the absolute value of all stiffness coefficients, damping coefficients and its growth rate increase with increasing eccentricity. The greater the eccentricity is, the stronger the hydrodynamic effect. Note that the larger the direct damping coefficients C_{xx} and C_{yy} are, the better the stability of the journal bearing in response to external disturbances. When the eccentricity is less than 0.5, the direct stiffness coefficients K_{xx} of the HGJB and PJB are approximately the same. Additionally, when the eccentricity is between 0.5-0.8, the direct stiffness coefficient K_{xx} of the HGJB is larger, while that of the PJB is larger when the eccentricity is larger than 0.8. The K_{yy} of the HGJB is greater than

that of the PJB at all eccentricities. When the eccentricity is larger than 0.5, the K_{xy} of the PJB is much greater than that of the HGJB. When the eccentricity is less than 0.5, it is approximately the same as that of the HGJB. When the eccentricity is less than 0.28, the C_{xx} of the HGJB is greater than that of the PJB. When the eccentricity is less than 0.58, the C_{yy} of the HGJB is greater than that of the PJB.

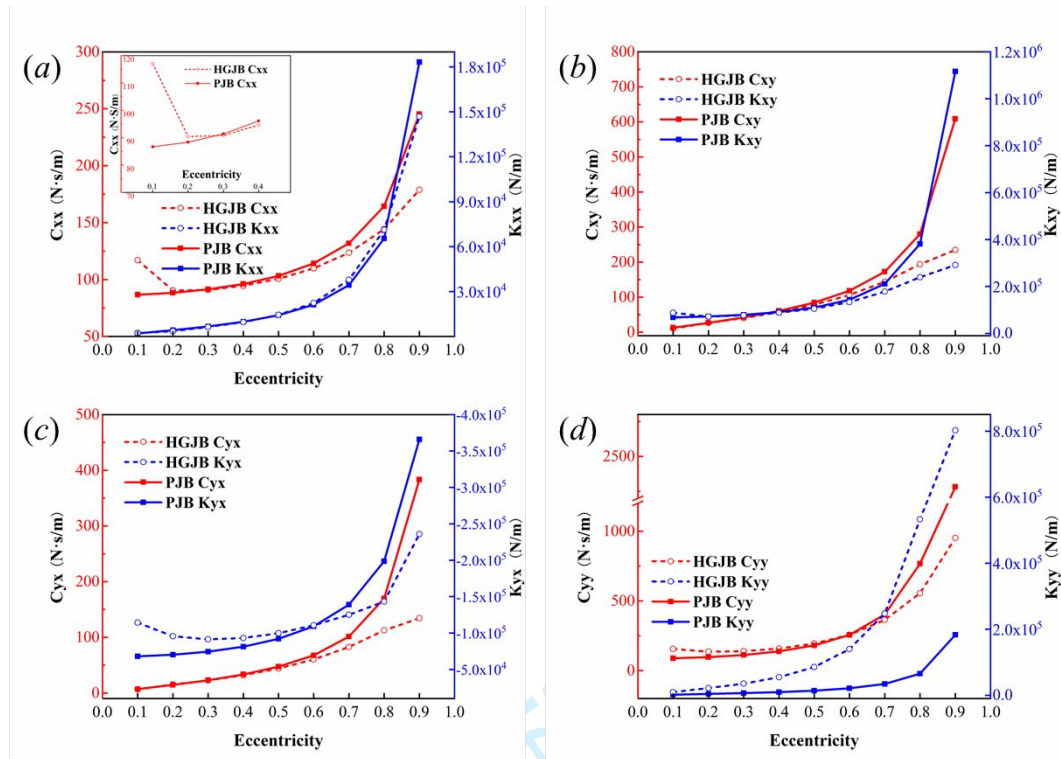


Fig. 8 Dynamic stiffness coefficients K_{ij} and damping coefficients C_{ij} of the HGJB and PJB varying with eccentricity.

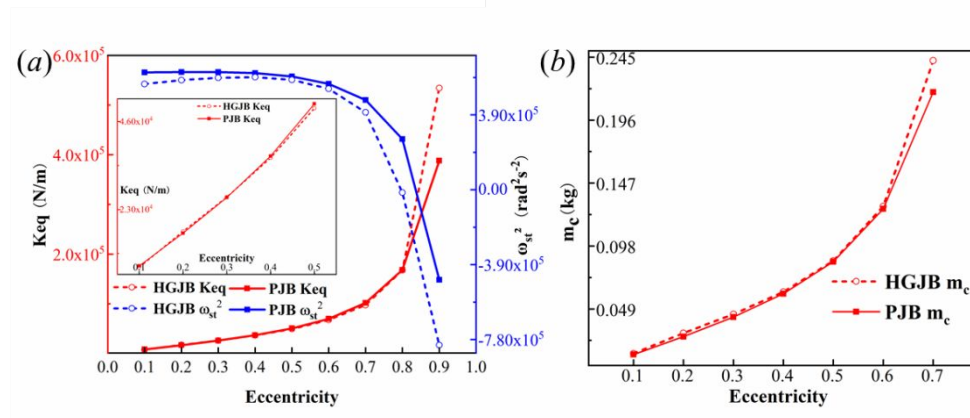


Fig. 9 (a) Equivalent stiffness coefficient K_{eq} and critical whirl frequency ω_{st} of the HGJB and PJB vary with eccentricity. (b) Critical journal masses (m_c) of the HGJB and PJB vary with eccentricity.

Fig. 9 (a) shows the variation in the equivalent stiffness coefficients and critical whirl frequency as the eccentricity varies. The results show that with increasing eccentricity, the K_{eq} of the HGJB and PJB increases, and ω_{st} decreases. Consequently, it can be concluded that with increasing eccentricity, the stability of the rotor-bearing system increases. More specifically, when the eccentricity is greater than

0.8, the K_{eq} of the HGJB is greater than that of the PJB. When the eccentricity is greater than 0.8, the ω_{st} of the HGJB becomes imaginary, which means that it reaches an absolutely stable state. The same is true for the PJB when the eccentricity is greater than 0.84. The ω_{st} of the HGJB is smaller than that of the PJB at all eccentricities. The abovementioned results show that the HGJB is more stable than the PJB in a certain range of eccentricity. To find this range precisely, the stabilities of both can be characterized by the critical journal mass m_c . As shown in Fig. 9 (b), when the eccentricity is less than 0.7, the m_c of the HGJB is larger than that of the PJB. This means that the HGJB is more stable than the PJB when the rotor mass is the same. When the eccentricity exceeds 0.84, the m_c of both become negative, and the systems reach stable states.

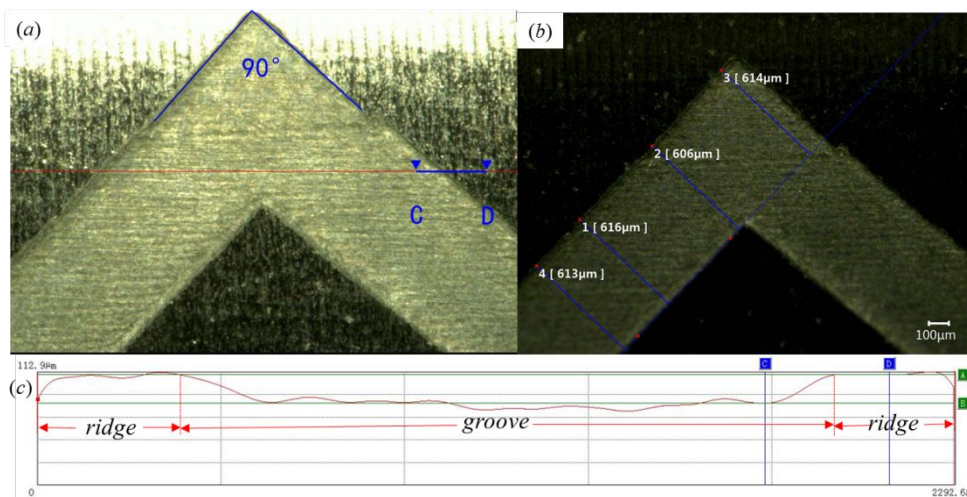


Fig. 10 (a) (b) Top view of the fabricated HGJB prototype, (c) absolute height distribution of the longitudinal section.

Fig. 10 shows the details of the HGJB we used in the experiment. As shown in Fig. 10, the HGJB was successfully fabricated by applying chemical etching technology. Fig. 10 (a) and (b) show the top view of the HGJB. The average width of the groove is 612.25 μm , which is slightly greater than the designed value of 600 μm , and the helix angle is 45°. To characterize the effective depth of the groove, an ultradepth three-dimensional micro-scope (Keyence, VHX-7000) was employed. The red line in Fig. 10 (a) represents the location of the longitudinal section, which spans the groove and the ridge. Fig. 10 (c) shows the absolute height distribution of the journal surface on the longitudinal section along the red line. The groove is approximately horizontal, and there is an obvious height difference between the groove and the ridge. By calculating the average height difference between the groove and the ridge, the depth of the groove is 28.54 μm .

To verify the conclusion of the numerical simulation, a laser displacement experiment is carried out. The journal radius used in the experiment is 6.33 mm, and the sleeve radius is 6.4 mm. The liquid lubricant is distilled water at 20°C, and the journal rotating speed is set to 15000 RPM. The sampling frequency of the laser displacement sensor is 20 kHz, and the time interval between adjacent sampling points is 50 μs . We measure the displacement of the journals in the X and Y directions, and 10000 data points are collected in each group.

Typically, as shown in Fig. 11, displacement–time responses within ten periods are selected for discussion. The amplitude and period of whirls of the HGJB and PJB are relatively fixed, but the absolute values of the peaks and valleys of each cycle are constantly changing, which indicates that the

whirl center is constantly changing. Moreover, the whirl amplitude of the journal of the PJB is larger than that of the HGJB, which indicates that the herringbone groove inhibits the whirl range of the rotor. The eccentricity variations in the journals in the above period are schematically shown in Fig. 11. The eccentricity is calculated as $e=r/c$. The calculation method of whirl radius r is as follows. It can be seen from Fig. 11 that both journals are moving elliptically around the origin of the sleeve. The HGJB has a smaller eccentricity, which is on average 16.87% less than that of the PJB.

$$r = \frac{1}{n} \sum_{i=1}^n \sqrt{\left(x_i - \frac{1}{n} \sum_{i=1}^n x_i\right)^2 + \left(y_i - \frac{1}{n} \sum_{i=1}^n y_i\right)^2} \quad (20)$$

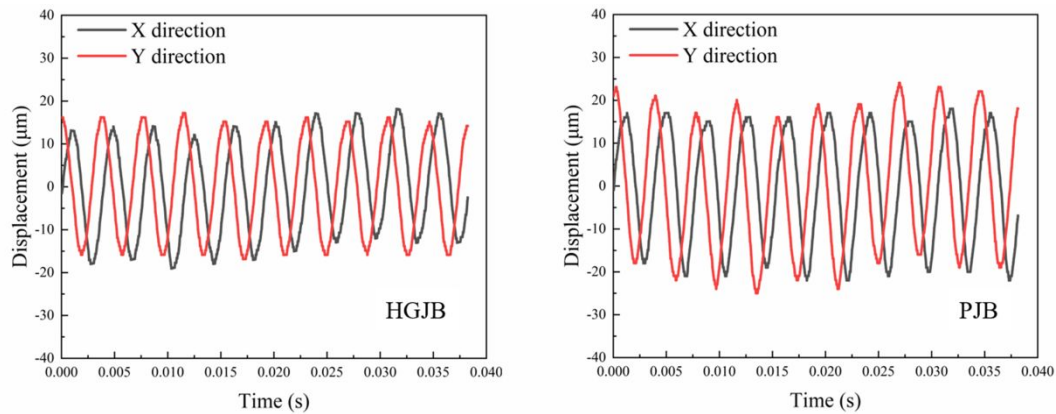


Fig. 11 Displacement in the X direction and Y direction of the HGJB and PJB.

From the initial analysis of Fig. 11, it can be inferred that the journal's whirl center is changing periodically. To investigate the regularity of the rotor's trajectory over a long period, the trajectory figure is drawn with a time interval of 0.5 s, as shown in Figs. 12 and 13. The whirl centers of the HGJB and PJB are constantly changing, but both are limited within a certain range. Moreover, the HGJB is more stable with its smaller whirl range. The long-term whirl amplitude of the HGJB in the X direction is $40.13 \mu\text{m}$, which is much lower than that of the PJB, which is $57.01 \mu\text{m}$. In the Y direction, the whirl amplitude of the HGJB is $37.98 \mu\text{m}$, which is much lower than that of the PJB, which is $50.03 \mu\text{m}$. The eccentricities of the HGJB and PJB within 0.5 seconds were calculated to be 0.222 and 0.276, respectively. From the above experimental test results, it can be observed that under the test conditions, the stability of the HGJB is better than that of the PJB, which is consistent with the results of the theoretical calculation.

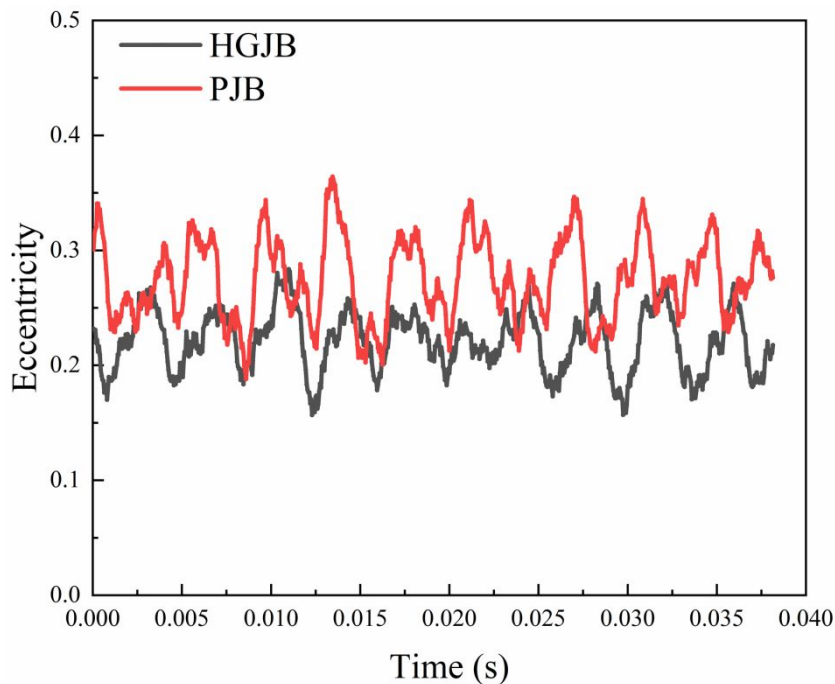


Fig. 12 Eccentricities of the HGJB and PJB vary with time.

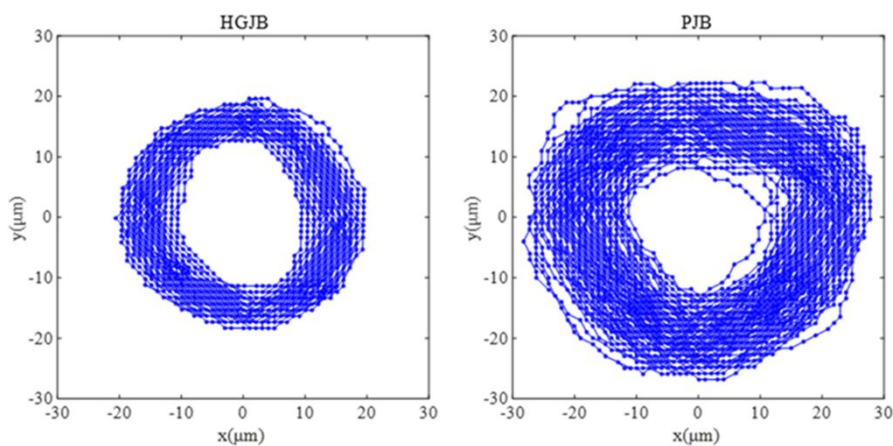


Fig. 13 Whirl trajectories of the HGJB and PJB within 0.5 s.

5. Conclusion

In this work, we developed a HGJB for the hydraulic suspension micro-pump. The CFD simulation and rotor dynamics calculation were combined to compare the dynamic and static characteristics of the HGJB and PJB. The results show that the HGJB has better working performance in a specific range of eccentricities, which can be explained by the pumping effect caused by the herringbone groove. Furthermore, the rotor dynamics calculation shows that the HGJB has better operational stability than the PJB when the eccentricity is less than 0.4 and greater than 0.62. We fabricated a prototype of the HGJB and established a set of laser displacement testing facilities to observe the trajectory of the journal in the HGJB and PJB. According to the experimental results, the operational stability of the HGJB is stronger than that of the PJB at the typical working speed of the micro-pump. The whirl range of the journal decreases by 29.61% in the X direction and by 24.09% in the Y direction. Therefore, it can be concluded that the herringbone grooved structure can significantly

1
2
3 suppress the whirl of the journal, reducing the risk of contact wear. HGJBs have a positive effect on
4 improving the operational stability of hydraulic suspension micro-pump.
5
6

7 **Acknowledgments**

8 This work was supported by the Open Fund of Science and Technology on Thermal Energy and
9 Power Laboratory (No. TPL 2019B03).
10
11
12
13
14
15
16
17
18
19
20
21
22
23
24
25

26 **References:**

- 27
28 [1] Nisar A, Afzulpurkar N, Mahaisavariya B. MEMS-based Micro-Pumps in Drug Delivery and
29 Biomedical Applications. *Sensors Actuat B-Chem*, 2008, 130: 917-942
30
31 [2] Tsai N C, Sue C Y. Review of MEMS-based Drug Delivery and Dosing Systems. *Sensor Actuat*
32 *A-Phys*, 2007, 2: 555-564
33
34 [3] Morshuis M, El-Banayosy A, Arusoglu L et al. European Experience of DuraHeart (TM)
35 Magnetically Levitated Centrifugal Left Ventricular Assist System. *Eur J Cardio-Thorac*, 2009, 6:
36 1020-1028
37
38 [4] Morshuis M, Schoenbrodt M, Nojiri C et al. DuraHeart (TM) Magnetically Levitated Centrifugal
39 Left Ventricular Assist System for Advanced Heart Failure Patients. *Expert Rev Med Devic*, 2010,
40 2: 173-183
41
42 [5] Luo X B, Hu R, Liu S et al. Heat and Fluid Flow in High-Power LED Packaging and Applications.
43 *Prog Energ Combust*, 2016, 1-32
44
45 [6] Wu R K, Fan Y W, Hong T et al. An Immersed Jet Array Impingement Cooling Device with
46 Distributed Returns for Direct Body Liquid Cooling of High Power Electronics. *Appl Therm Eng*,
47 2019, 162, 114259
48
49 [7] Liu P, Ren T, Ge Y et al. Performance Analyses of a Novel Finned Parabolic Trough Receiver
50 with Inner Tube for Solar Cascade Heat Collection. *Sci China Tech Sci*, 2023, 5: 1417-1434
51
52 [8] Zhang J, Chen Y, Liu Y et al. Experimental Investigation on Heat Transfer Characteristics of
53 Microcapsule Phase Change Material Suspension in Array Jet Impingement. *Sci China Tech Sci*,
54 2022, 7: 1634-1645
55
56 [9] Mohith S, Karanth P N, Kulkarni S M. Recent Trends in Mechanical Micropumps and Their
57 Applications: A Review. *Mechatronics*, 2019, 34-55
58
59 [10] Li H Y, Liu J K, Li K et al. A Review of Recent Studies on Piezoelectric Pumps and Their
60 Applications. *Mech Syst Signal Pr*, 2021, 151:107393
61
62 [11] Wang X Y, Cheng C, Wang S L et al. Electroosmotic Pumps and their Applications in

- 1
2
3 Microfluidic Systems. *Microfluid Nanofluid*, 2009, 2: 145-162
- 4 [12] Johnson M J, Go D B. Recent Advances in Electrohydrodynamic Pumps Operated by Ionic Winds:
5 A Review. *Plasma Sources Sci T*, 2017, 26: 103002
- 6 [13] Yang H, Jia H, Zhu Z C et al. Review of the Hydraulic and Structural Design of High-Speed
7 Centrifugal Pumps. *Front Energy Res*, 2022,10
- 8 [14] Wang C, Wang F, An D et al. A General Alternate Loading Technique and its Applications in the
9 Inverse Designs of Centrifugal and Mixed-Flow Pump Impellers. *Sci China Tech Sci*, 2021, 4:
10 898-918
- 11 [15] Yamane T. The Present and Future State of Nonpulsatile Artificial Heart Technology. *J Artif*
12 *Organs*, 2002, 5: 149-155
- 13 [16] Pagani F D. Continuous-Flow Rotary Left Ventricular Assist Devices with "3Rd Generation"
14 Design. *Semin Thorac Cardio*, 2008, 3: 255-263
- 15 [17] Kink T, Reul H. Concept for a New Hydrodynamic Blood Bearing for Miniature Blood Pumps.
16 *Artif Organs*, 2004, 10: 916-920
- 17 [18] Wu R K, Duan B, Liu F L et al. Design of a Hydro-Dynamically Levitated Centrifugal
18 Micro-Pump to the Active Liquid Cooling System. 18th International Conference on Electronic
19 Packaging Technology (ICEPT): 2017. 402-406
- 20 [19] Luo X B, Liu F L, Duan B et al. Micro Hydraulic Suspension Mechanical Pump. US patent:
21 10495093B2, 2017
- 22 [20] Kumar S, Kumar V, Singh A K. Influence of Lubricants on the Performance of Journal Bearings -
23 a Review. *Tribol-Mater Surf In*, 2020, 2: 67-78
- 24 [21] Garg H C, Sharda H B, Kumar V. On the Design and Development of Hybrid Journal Bearings: A
25 Review. *Tribotest*, 2006, 12: 1-19
- 26 [22] Tian L, Wang W J, Peng Z J. Nonlinear Effects of Unbalance in the Rotor-Floating Ring Bearing
27 System of Turbochargers. *Mech Syst Signal Pr*, 2013, 1-2: 298-320
- 28 [23] Chen S K, Chou H C, Kang Y. Stability Analysis of Hydrodynamic Bearing with Herringbone
29 Grooved Sleeve. *Tribol Int*, 2012, 15-28
- 30 [24] Gad A M, Nemat-Alla M M, Khalil A A et al. On the Optimum Groove Geometry for
31 Herringbone Grooved Journal Bearings. *J Tribol-T ASME*, 2006, 3: 585-593
- 32 [25] Ku R. Dynamic Characteristics of Hard Disk Drive Spindle Motors – Comparison Between Ball
33 Bearings and Hydrodynamic Bearings. *J Tribol-T ASME*, 1996, 118: 402-406
- 34 [26] Zhu J, Ono K. A Comparison Study on the Performance of Four Types of Oil Lubricated
35 Hydrodynamic Thrust Bearings for Hard Disk Spindles. *J Tribol-T ASME*, 1999, 121: 114-120
- 36 [27] Xu J, Jiao C, Zou D et al. Study on the Dynamic Behavior of Herringbone Gear Structure of
37 Marine Propulsion System Powered by Double-Cylinder Turbines. *Sci China Tech Sci*, 2022, 3:
38 611-630
- 39 [28] Hirayama T, Yamaguchi N, Sakai S et al. Optimization of Groove Dimensions in
40 Herringbone-Grooved Journal Bearings for Improved Repeatable Run-Out Characteristics. *Tribol*
41 *Int*, 2009, 5: 675-681
- 42 [29] Muijderman E A. Spiral Groove Bearings. *Ind Lubr Tribol*, 1965, 17: 12-17
- 43 [30] Chen S K, Chou H C, Kang Y. Stability Analysis of Hydrodynamic Bearing with Herringbone
44 Grooved Sleeve. *Tribol Int*, 2012, 15-28
- 45 [31] Sahu M, Sarangi M, Majumdar B C. Thermo-Hydrodynamic Analysis of Herringbone Grooved
46 Journal Bearings. *Tribol Int*, 2006, 11: 1395-1404
- 47
48
49
50
51
52
53
54
55
56
57
58
59
60

- 1
2
3
4 [32] Han Y, Xiong S, Wang J. A New Singularity Treatment Approach for Journal-Bearing Mixed
5 Lubrication Modeled by the Finite Difference Method with a Herring-Bone Mesh. *J Tribol-T*
6 *ASME*, 2016, 138 (1): 011704
7
8 [33] Zirkelback N, San Andres L. Finite Element Analysis of Herringbone Groove Journal Bearings: A
9 Parametric Study. *J Tribol-T ASME*, 1998, 2: 234-240
10
11 [34] Jang G H, Yoon J W. Nonlinear Dynamic Analysis of a Hydrodynamic Journal Bearing
12 Considering the Effect of a Rotating or Stationary Herringbone Groove. *J Tribol-T ASME*, 2002,
13 2: 297-304
14
15 [35] Hirs G G. The Load Capacity and Stability Characteristics of Hydrodynamic Grooved Journal
16 Bearings. *ASLE Trans*, 1965, 8: 296-305
17
18 [36] Gao S Y, Shi Y G, Xu L S et al. Investigation on Influences of Herringbone Grooves for the
19 Aerostatic Journal Bearings Applied to Ultra-High-Speed Spindles. *P I Mech Eng C-J Mec*, 2019,
20 16: 5795-5812
21
22 [37] Ikeda S, Arakawa Y, Hishida N et al. Herringbone-Grooved Bearing with Non-Uniform Grooves
23 for High-Speed Spindle. *Lubr Sci*, 2010, 9: 377-392
24
25 [38] Xing G Y, Xue S, Hong T et al. A Novel Hydrodynamic Suspension Micropump Using
26 Centrifugal Pressurization and the Wedge Effect. *Sci China Tech Sci*, 2023, (in pressed)
27
28 [39] Wang Bin, Sun Y T, Ding Q. Dynamic Characteristics of the Herringbone Groove Gas Journal
29 Bearings: Numerical Simulations. *Shock Vib*, 2016, 2016: 1-13
30
31 [40] Ingram T G. Stability of a Viscous Liquid Contained Between Two Rotating Cylinders. In, ed.
32 *Philosophical Transactions of the Royal Society of London*. London: 1923. 289-343
33
34 [41] Gao G, Yin Z, Jiang D et al. Numerical Analysis of Plain Journal Bearing under Hydrodynamic
35 Lubrication by Water. *Tribol Int*, 2014, 31-38
36
37 [42] Rowe W B, Chong F S. Computation of Dynamic Force Coefficients for Hybrid
38 (Hydrostatic/Hydrodynamic) Journal Bearings by the Finite Disturbance and Perturbation
39 Techniques. *Tribol Int*, 1986, 19: 260-271
40
41
42
43
44
45
46
47
48
49
50
51
52
53
54
55
56
57
58
59
60

Increasing operational stability of journal bearing in hydraulic suspension micro-pump by herringbone grooved structure

Tao Hong, Guanying Xing, Huaiyu Zuo, Song Xue, Xiaobing Luo*

State Key Laboratory of Coal Combustion, School of Energy and Power Engineering

Huazhong University of Science and Technology, Wuhan 430074, China

*luoxb@hust.edu.cn

Abstract

The operational stability of radial journal bearings is the bottleneck that limits the reliability of hydraulic suspension micro-pump. Due to self-excited vibrations, the whirl amplitude of the plain journal bearing (PJB) is large at high rotational speeds, which will accelerate wear failure. It has been proven that employing herringbone grooved journal bearing (HGJB) is an effective method to reduce the whirl amplitude and improve operational stability. However, enhancing the stability of journal bearings in micro-pumps by herringbone grooved structures has rarely been studied, and its effect needs to be verified. We validated the mechanism of the stability improvement with the CFD method and compared the dynamic characteristics of HGJB and PJB by rotor dynamics evaluation and experiment. The experimental results show that under the same conditions the whirl amplitude of the HGJB decreases by 29.61% in the X direction and by 24.09% in the Y direction compared with that of the PJB. This study reveals the effect of the herringbone grooved structure on the operational stability of bearings and may provide guidance for the reliability improvement of hydraulic suspension micro-pump.

Key words: journal bearing; herringbone groove; hydrodynamic effect; micro-pump.

1. Introduction

A micro-pump is the power source of microfluidic delivery, which is widely used in the fields of drug delivery [1, 2], artificial hearts [3, 4], electronic cooling systems [5-8], etc., and has broad application prospects [9]. According to the difference in working principles, micro-pumps can be divided into piezoelectric pumps [10], electroosmotic pumps [11], electrohydrodynamic pumps [12], and centrifugal pumps [13, 14]. Among them, centrifugal pumps have the advantages of high hydraulic performance and good adjustability, thus, they have become a promising choice for driving microfluidic systems. Centrifugal pumps can be divided into contact bearing pumps and suspension bearing pumps according to the supporting mode of the rotor [15, 16]. The problem of the contact bearing pump is mechanical friction, which restricts the reliability and endurance in application [16, 17]. To prevent contact wear problems, we developed a kind of hydraulic suspension micro-pump with a radial journal bearing in our previous works [18, 19]. The hydrodynamic effect makes the rotating components levitate, which prevents contact with other components, thus greatly improving the theoretical life of the micro-pump.

The radial suspension bearing used in this micro-pump is essentially a plain journal bearing (PJB), which is widely used in rotating machines. The journal is set eccentrically relative to the bearing, and the liquid film in the convergence zone produces a dynamic pressure effect when the journal rotates. This pressure balances the load on the journal and separates the journal from the inner wall of the bearing. However, the supporting force produced by the liquid film is not collinear with the eccentric direction of the journal, causing a moment that will promote the whirl of the journal. The moment will generate self-excited vibrations at high speeds, and the journal will no longer be in a steady state. As a result, when the whirl amplitude increases, collisions between the journal and bearing may occur, seriously affecting the performance and reliability of the pump. At present, researchers have carried out a series of studies

1
2
3 on increasing PJB operational stability. Kumar and Garg et al. found that the viscosity of the lubricant
4 has a significant influence on the dynamic characteristics of a PJB, and the use of magnetic fluids or
5 certain non-Newtonian fluids can improve the operational stability of a PJB [20, 21]. However, the fluid
6 choice depends on the function of the microfluidic system, making the viscosity change impractical.
7 Alternatively, adding external support, such as that used in floating ring bearings, provides an effective
8 means for increasing operational stability. The bearing is installed on the external film with appropriate
9 damping, which can absorb vibration energy and greatly reduce the whirl amplitude of the bearing [22].
10 However, external support will inevitably reduce the power density and increase the complexity of the
11 system. In addition, reducing the bearing width has also been proven to be an effective method to improve
12 operational stability [23]. Nonetheless, simply reducing the width will increase the end leakage and decay
13 the loading performance of the journal bearing. In addition, the motor design determines the width of the
14 rotor, thus limiting the structure optimization of the journal suspension. In summary, the three methods
15 mentioned above are not applicable in hydraulic suspension micro-pump. In recent years, the method of
16 machining microgrooves on the journal surface has become an effective means to improve the stability
17 of journal bearings due to its advantages of reliability and efficiency, which can improve operational
18 stability by strengthening the local hydrodynamic effect [24]. To date, grooved bearings have been widely
19 used in bearings with gas, liquid, and grease as lubricants, especially in miniaturized bearings [25-27].

20
21 Among the various shapes of grooves, the herringbone groove, which can suppress whirl instability,
22 has aroused widespread attention. The mechanism can be explained as follows: when the journal rotates,
23 the groove restricts the flow of fluids, which causes the fluids to converge at the cusp, forming a pumping
24 effect [24], thus enhancing the local pressure and improving the dynamic characteristics of the journal
25 bearing. Narrow groove theory (NGT) has been proposed to investigate the suspension characteristics of
26 a herringbone grooved journal bearing (HGJB) [28, 29], which assumes that the number of grooves is
27 infinite, while for an HGJB with finite slots, its accuracy is unsatisfying. Alternatively, the finite
28 difference method (FDM) [30-32] and finite element method (FEM) [33, 34] are used to solve the nonlinear
29 Reynolds equation numerically and are sufficiently accurate compared to the experiments. Furthermore,
30 Hirs [35] and Gao [36] experimentally studied a hydrodynamic HGJB and an aerostatic HGJB and obtained
31 better stability compared to a PJB. In addition, an HGJB can significantly restrain the radial runout of
32 the high-speed spindle and increase the maximum operating speed [37]. Due to its excellent dynamic
33 properties, HGJBs have been used in high-speed light-load rotating machinery, such as high-precision
34 machine tool spindles and hard disks. Moreover, there are few studies that use herringbone grooves to
35 improve the stability of radial suspension bearings in micro-pump. Inspired by this, we employ an HGJB
36 to improve the operational stability of the micro-pump, conduct theoretical modeling and analysis to
37 explore its dynamic and static characteristics, and verify its effect by experiments.

38
39 In this work, we developed a herringbone grooved structure on a journal bearing applied in a micro-
40 pump. The comprehensive effect of herringbone grooves on water-lubricated journal bearings is studied
41 numerically and experimentally. By CFD simulation, the pressure distribution and bearing capacity of
42 the HGJB and PJB at different eccentricities are studied comparatively. Moreover, based on the
43 perturbation method, the stiffness and damping coefficients are solved to clarify the rotor dynamic
44 characteristics. Then, the critical mass is obtained by solving the rigid body motion equation, and the
45 stability of the HGJB and PJB is evaluated. Finally, the veracity of the theoretical analysis is verified by
46 experiments.

47 48 49 50 51 52 53 54 55 56 57 58 **2. Operating Principle of the Hydraulic Suspension Micro-pump with the PJB and the HGJB**

59 Fig. 1 shows the structure of the hydraulic suspension micro-pump with the radial suspension
60

bearing proposed in our previous work [18, 19, 38]. The journal bearing is composed of a rotor inside a sleeve, with a small clearance between them for fluid flow. Due to the eccentric placement of the journal, when the journal rotates, the thickness of the liquid film changes along the direction of rotation, forming a convergent region (part I in Fig. 1) on the right side of line OO_1 and a diverging region (part II in Fig. 1) on the left side. Due to the hydrodynamic effect, the liquid film of the convergent region generates high pressure, and the pressure of the diverging region decreases rapidly, thus constructing the pressure difference between the two regions and providing the radial suspension force.

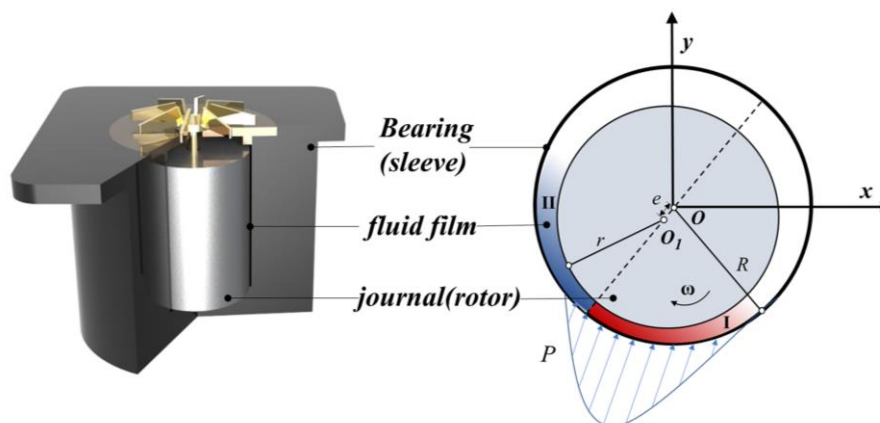


Fig. 1 Schematic diagram of the journal bearing in the hydraulic suspension micro-pump

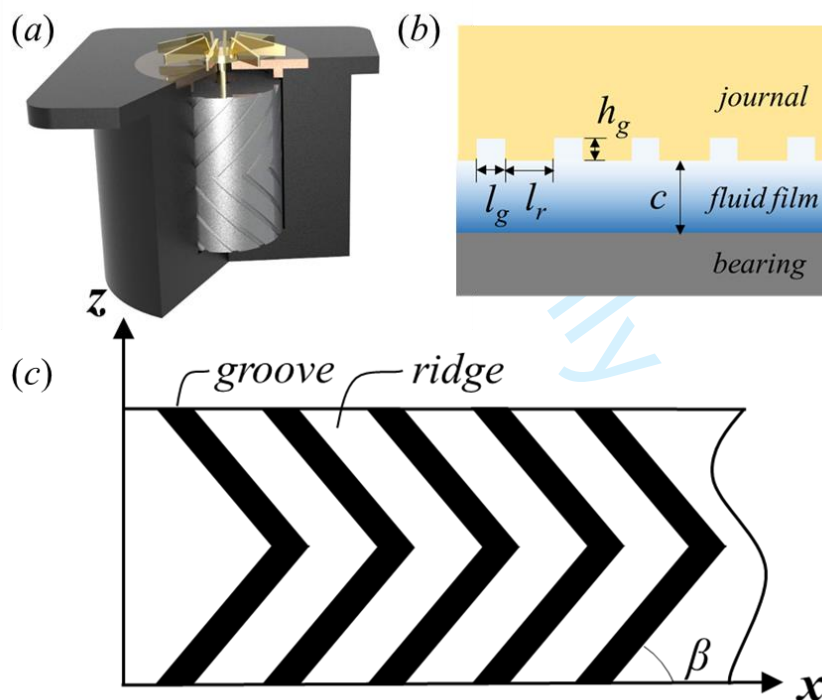


Fig. 2 (a) 3D rendered graph of the HGJB in a micro-pump. (b) cross-sectional view of the HGJB.

(c) Radial expansion diagram of the herringbone grooved structure.

The HGJB employed in this paper has a rectangular section, and the structure of the HGJB is shown in Fig. 2. The main structural parameters are shown in Table 1, where the groove number $n=12$, helix angle $\beta=45^\circ$, groove width $l_g=0.6$ mm and groove depth $h_g=28.5$ μm . It should be mentioned that the

values of the groove number and helix angle are referred to Bin Wang's work [39], and the depth and width of the groove are determined by the machining precision. Thus, we believe that the working performance of the HGJB may be better if the geometrical parameters are optimized further.

Table 1 Structure parameters of the PJB and HGJB.

Type	length l (mm)	radius r (mm)	clearance c (mm)	n	β (°)	l_g (mm)	h_g (μm)
PJB	17.2	6.33	0.07	/	/	/	/
HGJB	17.2	6.33	0.07	12	45	0.6	28.5

3. Methods

3.1 Experimental Setup

Distinctly, the stability of journal bearings can be reflected by the journal's whirl tail. To observe it accurately, a test facility is constructed, and Fig. 3 (a) shows the overall schematic diagram of the test facility. To measure the real-time position of the journal, two laser displacement sensors (Keyence, LK-H020) with $\pm 1 \mu\text{m}$ accuracy are installed on two micro-displacement stages (LD60-LM-2). The HGJB is assembled into a micro-pump with acrylic volute, whose transmissivity is high (more than 90%), allowing the laser to flash on the bearing. The inlet and outlet tubes of the micro-pump are connected to a water sink. To reduce the interference of external vibrations and ensure sufficient levelness, the working micro-pump is installed on a specific fixture, and the entire test facility is installed on a high-precision optical platform.

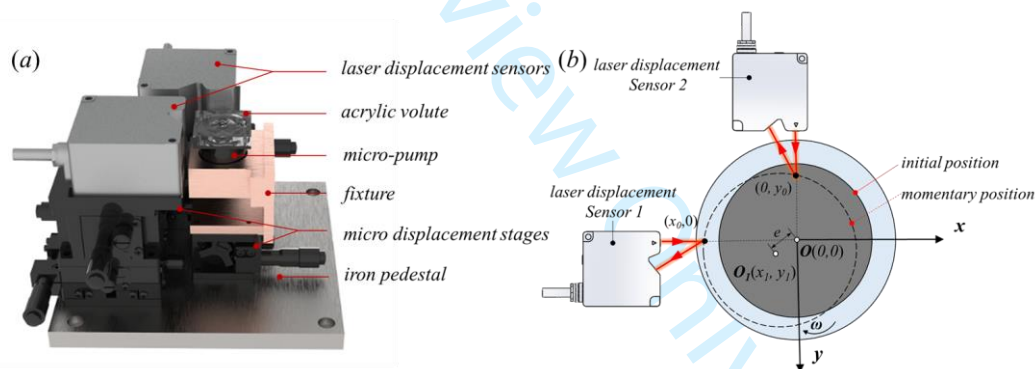


Fig. 3 (a) Overall schematic diagram of the test facility. (b) Schematic diagram of the experimental test principle.

The test principle in this work is shown in Fig. 3 (b). Two laser displacement sensors are arranged vertically in the radial direction of the micro-pump. The laser flashes on the journal through the acrylic volute, and then the reflected light returns to the receiver. The data x_0 and y_0 are directly recorded by laser displacement sensors. The momentary position (x_1, y_1) of the rotor can be calculated by combining Eq. (1) and (2), and the eccentricity e is denoted below.

$$(x_0 - x_1)^2 + (0 - y_1)^2 = r^2 \quad (1)$$

$$(0 - x_1)^2 + (y_0 - y_1)^2 = r^2 \quad (2)$$

$$e = \sqrt{x_1^2 + x_2^2} \quad (3)$$

3.2 Numerical Simulation

Numerical simulations are conducted to investigate the dynamic coefficients and pressure distributions of the HGJB and the PJB by using COMSOL MULTIPHYSICS 5.6. Fig. 4 shows the journal film domains of the PJB and the HGJB used in the simulation. Structured meshes are used for the PJB, and unstructured meshes are used for the HGJB. As shown in Fig. 4, to capture the fluid flow process and pressure distribution details, grids are meshed finer in the herringbone groove zone. The pressure boundary condition of the inlet and outlet is set to zero pressure. The flow state of the liquid is judged by the critical Reynolds number formula of the concentric cylinder in Eq. (4) [40]. The Reynolds numbers of the PJB and HGJB are calculated as follows.

$$Re_c = 41.1\sqrt{\frac{R}{C}} \quad (4)$$

$$Re = \frac{\rho ud}{\mu} \quad (5)$$

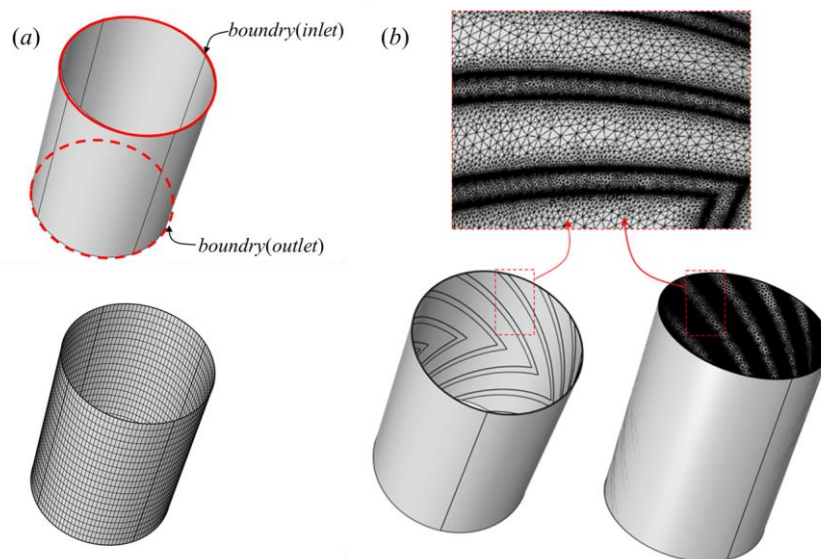


Fig. 4 Simulation models of the PJB (a) and the HGJB (b).

In this simulation, 20°C water is used as lubricant, and the density and dynamic viscosity are set to 998.2 kg/m³ and 1.006 mPa·s, respectively. The grid independence tests are performed at a rotating speed of 15000 RPM and eccentricity of 0.1. The maximum pressures of the HGJB are calculated with grid numbers of 41836, 132184, 443867, and 737229. The results are shown in Table 2. Similarly, the grid independence results of the PJB are shown in Table 2 too. Taking computation cost into consideration, the mesh scheme with a grid number of 443867 is used for the HGJB, while a grid number of 2400 is used for the PJB.

Table 2 Grid independence verification results of the HGJB and PJB.

HGJB	Grid number	41836	132184	443867	737229
	Max pressure	6066.5	6069.8	6074.9	6077.1
PJB	Grid number	2400	3200	4800	6400
	Max pressure	3170.6	3170.6	3170.6	3170.6

3.3 Numerical Method Verification

Based on the numerical simulation method mentioned earlier, the performance of journal bearings is studied. To validate this method, six cases are studied, and the numerical results are compared with the experimental data of Gao and Yin's work [41].

Gao and Yin's experiment used 20°C water as lubricant to test the eccentricity of bearings under six working conditions, as listed in Table 3, including different rotating speeds and loads. Fig. 5 is a comparison of the numerical calculation results and Gao and Yin's experimental data under six working conditions. The results show that the numerical calculation results match well with the experimental data, and the maximum error is less than 8.45%.

Table 3 Working conditions of Gao and Yin's experiment.

Case	Rotating speed	Load
1	1500 RPM	2050 N
2	2000 RPM	2700 N
3	2500 RPM	3350 N
4	3000 RPM	3950 N
5	3500 RPM	4850 N
6	4000 RPM	5200 N

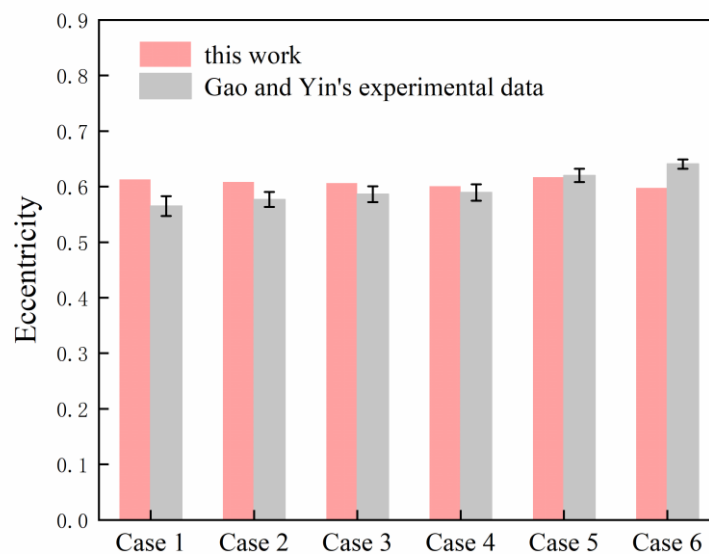


Fig. 5 Simulation model of the PJB (a) and the HGJB (b).

3.4 Rotor Dynamic Calculation

From the viewpoint of rotor dynamics, the liquid film usually acts as a nonlinear spring and damper, which has a great influence on the dynamic characteristics of the whole system. In the study of journal bearings, because most of them involve only small or infinitesimal amplitudes, the stiffness coefficient and damping characteristics of the liquid film are considered to be linear.

Assuming that the journal is in static equilibrium, a Taylor expansion is carried out for the bearing

capacity in the x and y directions. After ignoring higher-order terms, the bearing capacity is given as follows:

$$\begin{aligned} F_x &= F_{x0} + \left(\frac{\partial F_x}{\partial x} \right)_0 \Delta x + \left(\frac{\partial F_x}{x \partial y} \right)_0 x \Delta y + \left(\frac{\partial F_x}{\partial x'} \right)_0 x' + \left(\frac{\partial F_x}{x \partial y'} \right)_0 xy' \\ F_y &= F_{y0} + \left(\frac{\partial F_y}{\partial x} \right)_0 \Delta x + \left(\frac{\partial F_y}{x \partial y} \right)_0 x \Delta y + \left(\frac{\partial F_y}{\partial x'} \right)_0 x' + \left(\frac{\partial F_y}{x \partial y'} \right)_0 xy' \end{aligned} \quad (6)$$

It can be seen that the coefficient of the original term in Eq. (6) has a stiffness dimension, and the coefficient of the first-order term has a damping dimension. After simplification, it can be expressed by Eq. (7)

$$\begin{pmatrix} \Delta F_x \\ \Delta F_y \end{pmatrix} = \begin{pmatrix} K_{xx} & K_{xy} \\ K_{yx} & K_{yy} \end{pmatrix} \begin{pmatrix} \Delta x \\ \Delta y \end{pmatrix} + \begin{pmatrix} C_{xx} & C_{xy} \\ C_{yx} & C_{yy} \end{pmatrix} \begin{pmatrix} x' \\ y' \end{pmatrix} \quad (7)$$

where K_{xx} and K_{yy} are direct stiffness coefficients, K_{xy} and K_{yx} are cross stiffness coefficients, C_{xx} and C_{yy} are direct damping coefficients, C_{xy} and C_{yx} are cross damping coefficients, Δx and Δy are displacements, and x' and y' are the velocities. The dynamic characteristics of the HGJB and the PJB are calculated by the pressure perturbation method^[42]. The calculation method is denoted as follows:

$$K_{xx} = \frac{\Delta F_{sxx}}{\Delta x} \quad K_{xy} = \frac{\Delta F_{sxy}}{\Delta y} \quad K_{yx} = \frac{\Delta F_{syx}}{\Delta x} \quad K_{yy} = \frac{\Delta F_{syy}}{\Delta y} \quad (8)$$

$$C_{xx} = \frac{\Delta F_{vxx}}{x'} \quad C_{xy} = \frac{\Delta F_{vxy}}{y'} \quad C_{yx} = \frac{\Delta F_{vyx}}{x'} \quad C_{yy} = \frac{\Delta F_{vyy}}{y'} \quad (9)$$

In Eq. (8), ΔF_{sij} is the variation in fluid film capacity caused by displacement perturbation, $\Delta F_{sij} = F_{sij} - F'_{sij}$, where F_{sij} is the liquid film capacity in the equilibrium state, and F'_{sij} is the liquid film capacity after the displacement perturbation is applied. In Eq. (9), ΔF_{vij} is the variation in the fluid film capacity caused by the velocity perturbation. $\Delta F_{vij} = F_{vij} - F'_{vij}$, where F_{vij} is the liquid film capacity in the equilibrium state, and F'_{vij} is the liquid film capacity after the velocity perturbation is applied.

The dynamic characteristic parameters of liquid films are very important for studying the stability of journal bearings. Generally, the larger the stiffness of the liquid film is, the stronger the bearing capacity, and the larger the damping is, the better the stability. Furthermore, the influence of stiffness and damping need to be considered simultaneously when studying the stability of a journal bearing, and the optimization approach must be based on the coupling effect between them to achieve the best stability. The system stability is characterized by the critical journal mass, which is determined by the stiffness coefficient, damping coefficient and journal mass. By substituting Eq. (6) into instantaneous dynamic Eq. (10),

$$\begin{aligned} mx'' + \Delta F_x &= 0 \\ my'' + \Delta F_y &= 0 \end{aligned} \quad (10)$$

The dynamical equation of journal bearings can be expressed as Eq. (11):

$$\begin{aligned} mx'' + K_{xx} \Delta x + K_{xy} \Delta y + C_{xx} x' + C_{xy} y' &= 0 \\ my'' + K_{yx} \Delta x + K_{yy} \Delta y + C_{yx} x' + C_{yy} y' &= 0 \end{aligned} \quad (11)$$

Eq. (11) is a linear equation whose general solution is shown below, where v is the eigenvalue and is

a complex number.

$$\begin{aligned}\Delta x &= x_0 e^{v t} \\ \Delta y &= y_0 e^{v t}\end{aligned}\quad (12)$$

By substituting Eq. (12) into Eq. (11), the characteristic equation is given as:

$$\begin{aligned}(m v^2 + C_{xx} v + K_{xx}) x_0 + (C_{xy} v + K_{xy}) y_0 &= 0 \\ (C_{yx} v + K_{yx}) x_0 + (m v^2 + C_{yy} v + K_{yy}) y_0 &= 0\end{aligned}\quad (13)$$

In the critical state, there exists an eigenvalue v that is a pure imaginary number. Here, $v = i\omega_{st}$, and v is substituted into Eq. (10); it can be expressed as:

$$\begin{aligned}\Delta F_x &= m\omega_{st}^2 x_0 e^{i\omega_{st} t} = m\omega_{st}^2 \Delta x \\ \Delta F_y &= m\omega_{st}^2 y_0 e^{i\omega_{st} t} = m\omega_{st}^2 \Delta y\end{aligned}\quad (14)$$

where ω_{st} is the critical whirl frequency. In the critical state, the proportional coefficient between ΔF_x and Δx , ΔF_y and Δy is $m\omega_{st}^2$. This indicates that the liquid film at this time is equivalent to an isotropic spring with similar dynamic characteristics, and its stiffness is called the equivalent stiffness, which is expressed by K_{eq} as follows:

$$K_{eq} = m\omega_{st}^2 \quad (15)$$

By substituting Eq. (15) and $v = i\omega_{st}$ into Eq. (13), we obtain:

$$\begin{aligned}(i\omega_{st} C_{xx} + K_{xx} - K_{eq}) x_0 + (i\omega_{st} C_{xy} + K_{xy}) y_0 &= 0 \\ (i\omega_{st} C_{yx} + K_{yx}) x_0 + (i\omega_{st} C_{yy} + K_{yy} - K_{eq}) y_0 &= 0\end{aligned}\quad (16)$$

For Eq. (16), only when a nontrivial solution exists will the determinant of the coefficients equal 0. Then, the motion of the rotor converges. The convergence criterion of the rotor can be expressed as follows:

$$\begin{vmatrix} i\omega_{st} C_{xx} + K_{xx} - K_{eq} & i\omega_{st} C_{xy} + K_{xy} \\ i\omega_{st} C_{yx} + K_{yx} & i\omega_{st} C_{yy} + K_{yy} - K_{eq} \end{vmatrix} = 0 \quad (17)$$

where the equivalent stiffness K_{eq} and the critical whirl frequency ω_{st} can be obtained by expanding the determinant:

$$\begin{aligned}K_{eq} &= \frac{K_{xx} C_{yy} + K_{yy} C_{xx} - K_{xy} C_{yx} - K_{yx} C_{xy}}{C_{xx} + C_{yy}} \\ \omega_{st}^2 &= \frac{(K_{eq} - K_{xx})(K_{eq} - K_{yy}) - K_{xy} K_{yx}}{C_{xx} C_{yy} - C_{xy} C_{yx}}\end{aligned}\quad (18)$$

where K_{eq} reflects the comprehensive stiffness of the liquid film and ω_{st} reflects the development degree of whirl in the liquid film. When the other conditions are consistent, if K_{eq} is larger and ω_{st} is smaller, the stability of the rotor-bearing system is better. Obviously, the equivalent stiffness coefficient of the liquid film should always be greater than zero, and $K_{eq} > 0$ is a necessary condition for system stability. When $\omega_{st} < 0$, even if a perturbation is applied, the whirl will decay quickly; hence, $\omega_{st} < 0$ is the sufficient condition for system stability. Only when $K_{eq} > 0$ and $\omega_{st} > 0$ does the system seem to be unstable. As follows, the ratio of K_{eq} to ω_{st}^2 is the critical journal mass, which is the key indicator for system stability.

$$m_c = \frac{K_{eq}}{\omega_{st}^2} \quad (19)$$

If the actual mass of the rotor is greater than m_c , the rotor motion is divergent, and the system is unstable. In contrast, the rotor motion is convergent, and the system is stable. Furthermore, the larger m_c is, the higher the stability margin of the system is.

4. Results and Discussion

Simulations are carried out at 15000 RPM, which is the typical working speed of this micro-pump. The pressure distribution, bearing capacity and dynamic coefficients of the HGJB and PJB when the eccentricity is 0.1-0.9 are investigated by numerical simulations. Taking the eccentricity of 0.1 as an example, the pressure distribution of the HGJB and PJB are shown in Fig. 6 (a). It can be observed that the hydrodynamic effect of fluid causes a positive-pressure region and a negative-pressure region on the journal surface. It is evident that HGJB produces a higher pressure at the cusp of the herringbone groove than the same position of the PJB. Fig. 6 (b) shows the pressure distribution of the intermediate plane on the HGJB and PJB. The maximum and minimum pressures of the PJB are 3170.7 Pa and -3170.7 Pa, which are symmetrically distributed in the convergent region and diverging region, respectively. The maximum pressure of the HGJB is 8096 Pa, and the minimum pressure is -1784 Pa. There are twelve pressure peaks on the HGJB, which correspond to twelve herringbone grooves on the journal surface. The reason for this phenomenon is that the herringbone grooves restrict the fluid flow in the bearing clearance, and the fluid converges at the cusps, making the local pressure higher than

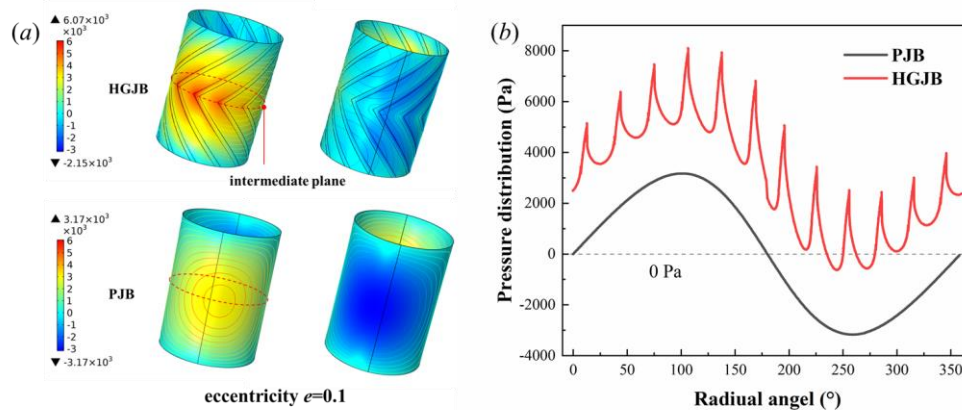


Fig. 6 (a) Pressure distribution contours of the HGJB and PJB.

(b) Pressure distribution on the intermediate circle of the HGJB and PJB varies with radial angle.

As shown in Fig. 7, with increasing eccentricity, the bearing capacity and maximum pressure of the HGJB and PJB increase sharply, while the minimum pressure decreases sharply. When the eccentricity increases, the minimum thickness of the liquid film decreases, and the gradient of the liquid film thickness in the bearing clearance increases, which enhances the hydrodynamic effect of the fluid. As a result, the pressure in the convergent region is higher, the pressure in the diverging region is lower, and the loading capacity is larger. The results show that when the eccentricity is less than 0.55, the minimum pressure of the HGJB is greater than that of the PJB, and the maximum pressure of the HGJB is always greater than that of the PJB. This indicates that the fluid pumping effect brought by the herringbone grooves enhance the positive pressure. Moreover, the force of the convergent region is enhanced while

that of the diverging region is weakened. When the eccentricity is less than 0.74, the load capacity of the HGJB is greater than that of the PJB, and it is smaller than that of the PJB when the eccentricity is larger than 0.74. The reason for this phenomenon is that when the eccentricity is at the critical value of 0.74, the strengthening of the force in the convergent region will offset the weakening of the force in the diverging region, making the bearing capacity of the HGJB equal to PJB.

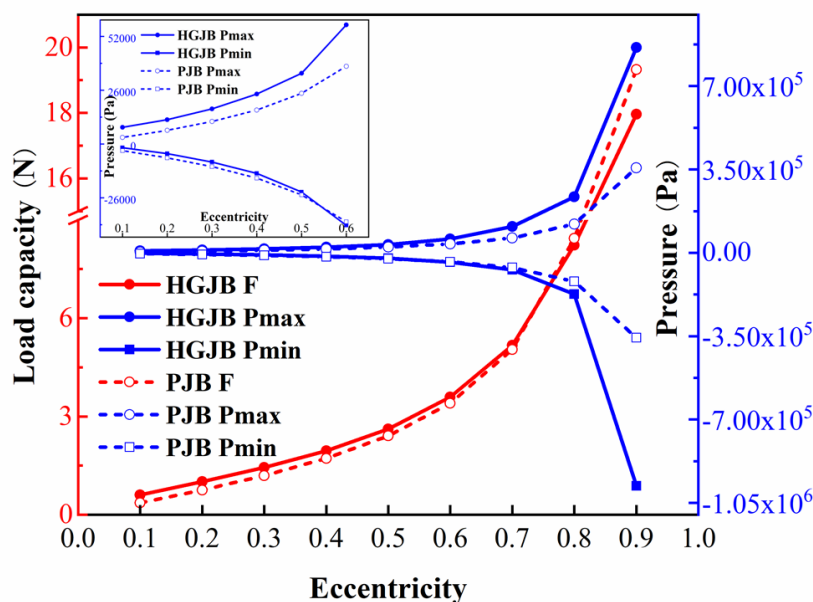


Fig. 7 Journal bearing capacity and the maximum/ minimum pressure of the HGJB and PJB vary with eccentricity.

Fig. 8 shows the variation in the stiffness coefficients and damping coefficients as the eccentricity varies. The results show that the absolute value of all stiffness coefficients, damping coefficients and its growth rate increase with increasing eccentricity. The greater the eccentricity is, the stronger the hydrodynamic effect. Note that the larger the direct damping coefficients C_{xx} and C_{yy} are, the better the stability of the journal bearing in response to external disturbances. When the eccentricity is less than 0.5, the direct stiffness coefficients K_{xx} of the HGJB and PJB are approximately the same. Additionally, when the eccentricity is between 0.5-0.8, the direct stiffness coefficient K_{xx} of the HGJB is larger, while that of the PJB is larger when the eccentricity is larger than 0.8. The K_{yy} of the HGJB is greater than that of the PJB at all eccentricities. When the eccentricity is larger than 0.5, the K_{yy} of the PJB is much greater than that of the HGJB. When the eccentricity is less than 0.5, it is approximately the same as that of the HGJB. When the eccentricity is less than 0.28, the C_{xx} of the HGJB is greater than that of the PJB. When the eccentricity is less than 0.58, the C_{yy} of the HGJB is greater than that of the PJB.

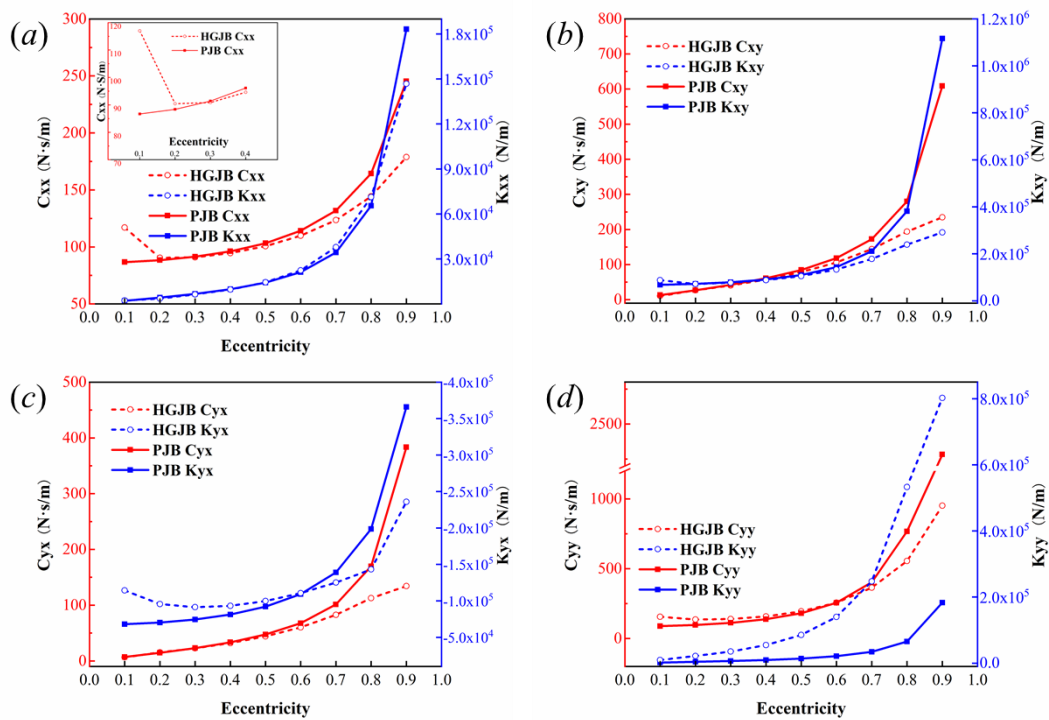


Fig. 8 Dynamic stiffness coefficients K_{ij} and damping coefficients C_{ij} of the HGJB and PJB varying with eccentricity.

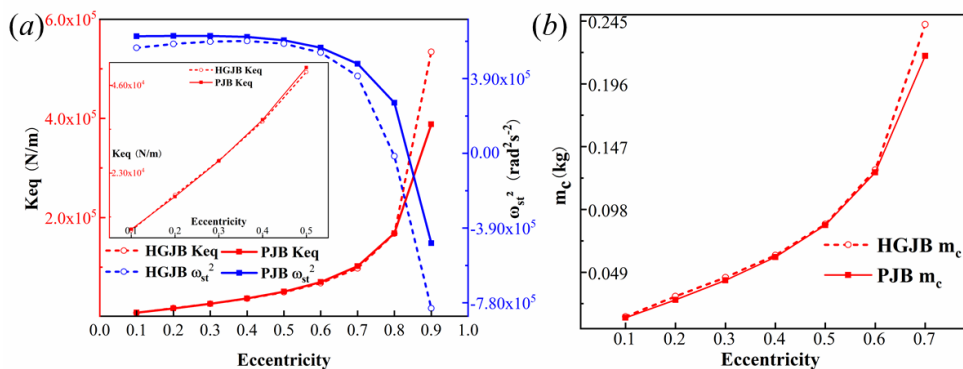


Fig. 9 (a) Equivalent stiffness coefficient K_{eq} and critical whirl frequency ω_{st} of the HGJB and PJB vary with eccentricity. (b) Critical journal masses (m_c) of the HGJB and PJB vary with eccentricity.

Fig. 9 (a) shows the variation in the equivalent stiffness coefficients and critical whirl frequency as the eccentricity varies. The results show that with increasing eccentricity, the K_{eq} of the HGJB and PJB increases, and ω_{st} decreases. Consequently, it can be concluded that with increasing eccentricity, the stability of the rotor-bearing system increases. More specifically, when the eccentricity is greater than 0.8, the K_{eq} of the HGJB is greater than that of the PJB. When the eccentricity is greater than 0.8, the ω_{st} of the HGJB becomes imaginary, which means that it reaches an absolutely stable state. The same is true for the PJB when the eccentricity is greater than 0.84. The ω_{st} of the HGJB is smaller than that of the PJB at all eccentricities. The abovementioned results show that the HGJB is more stable than the PJB in a

certain range of eccentricity. To find this range precisely, the stabilities of both can be characterized by the critical journal mass m_c . As shown in Fig. 9 (b), when the eccentricity is less than 0.7, the m_c of the HGJB is larger than that of the PJB. This means that the HGJB is more stable than the PJB when the rotor mass is the same. When the eccentricity exceeds 0.84, the m_c of both become negative, and the systems reach stable states.

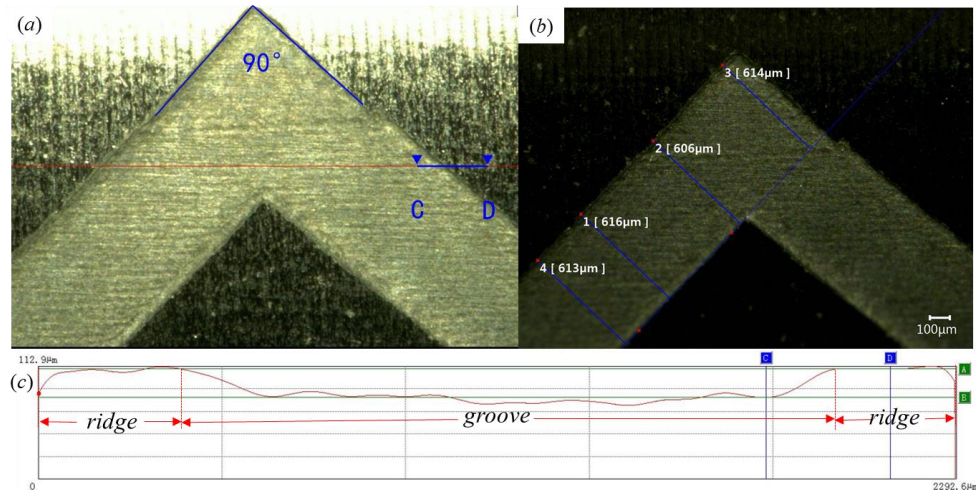


Fig. 10 (a) (b) Top view of the fabricated HGJB prototype, (c) absolute height distribution of the longitudinal section.

Fig. 10 shows the details of the HGJB we used in the experiment. As shown in Fig. 10, the HGJB was successfully fabricated by applying chemical etching technology. Fig. 10 (a) and (b) show the top view of the HGJB. The average width of the groove is $612.25 \mu\text{m}$, which is slightly greater than the designed value of $600 \mu\text{m}$, and the helix angle is 45° . To characterize the effective depth of the groove, an ultradepth three-dimensional micro-scope (Keyence, VHX-7000) was employed. The red line in Fig. 10 (a) represents the location of the longitudinal section, which spans the groove and the ridge. Fig. 10 (c) shows the absolute height distribution of the journal surface on the longitudinal section along the red line. The groove is approximately horizontal, and there is an obvious height difference between the groove and the ridge. By calculating the average height difference between the groove and the ridge, the depth of the groove is $28.54 \mu\text{m}$.

To verify the conclusion of the numerical simulation, a laser displacement experiment is carried out. The journal radius used in the experiment is 6.33 mm , and the sleeve radius is 6.4 mm . The liquid lubricant is distilled water at 20°C , and the journal rotating speed is set to 15000 RPM . The sampling frequency of the laser displacement sensor is 20 kHz , and the time interval between adjacent sampling points is $50 \mu\text{s}$. We measure the displacement of the journals in the X and Y directions, and 10000 data points are collected in each group.

Typically, as shown in Fig. 11, displacement–time responses within ten periods are selected for discussion. The amplitude and period of whirls of the HGJB and PJB are relatively fixed, but the absolute values of the peaks and valleys of each cycle are constantly changing, which indicates that the whirl center is constantly changing. Moreover, the whirl amplitude of the journal of the PJB is larger than that of the HGJB, which indicates that the herringbone groove inhibits the whirl range of the rotor. The eccentricity variations in the journals in the above period are schematically shown in Fig. 11. The eccentricity is calculated as $e=r/c$. The calculation method of whirl radius r is as follows. It can be seen

from Fig. 11 that both journals are moving elliptically around the origin of the sleeve. The HGJB has a smaller eccentricity, which is on average 16.87% less than that of the PJB.

$$r = \frac{1}{n} \sum_1^n \sqrt{\left(x_i - \frac{1}{n} \sum_1^n x_i\right)^2 + \left(y_i - \frac{1}{n} \sum_1^n y_i\right)^2} \quad (20)$$

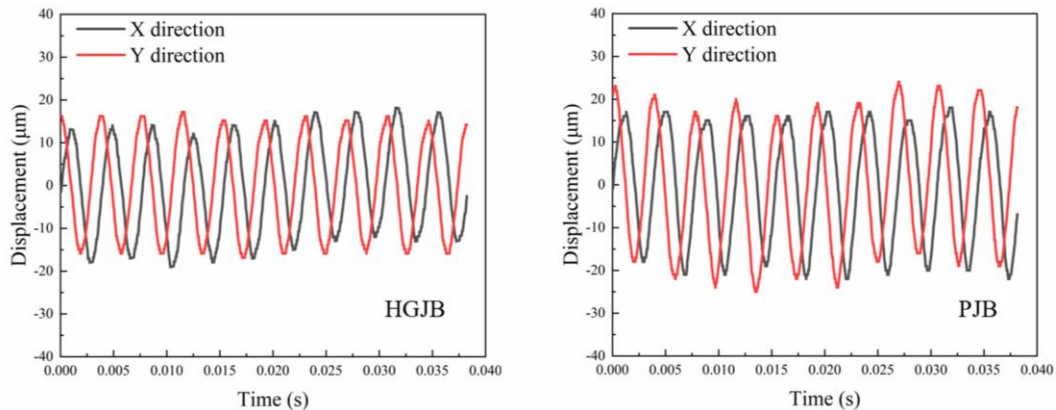


Fig. 11 Displacement in the X direction and Y direction of the HGJB and PJB.

From the initial analysis of Fig. 11, it can be inferred that the journal's whirl center is changing periodically. To investigate the regularity of the rotor's trajectory over a long period, the trajectory figure is drawn with a time interval of 0.5 s, as shown in Figs. 12 and 13. The whirl centers of the HGJB and PJB are constantly changing, but both are limited within a certain range. Moreover, the HGJB is more stable with its smaller whirl range. The long-term whirl amplitude of the HGJB in the X direction is 40.13 μm , which is much lower than that of the PJB, which is 57.01 μm . In the Y direction, the whirl amplitude of the HGJB is 37.98 μm , which is much lower than that of the PJB, which is 50.03 μm . The eccentricities of the HGJB and PJB within 0.5 seconds were calculated to be 0.222 and 0.276, respectively. From the above experimental test results, it can be observed that under the test conditions, the stability of the HGJB is better than that of the PJB, which is consistent with the results of the theoretical calculation.

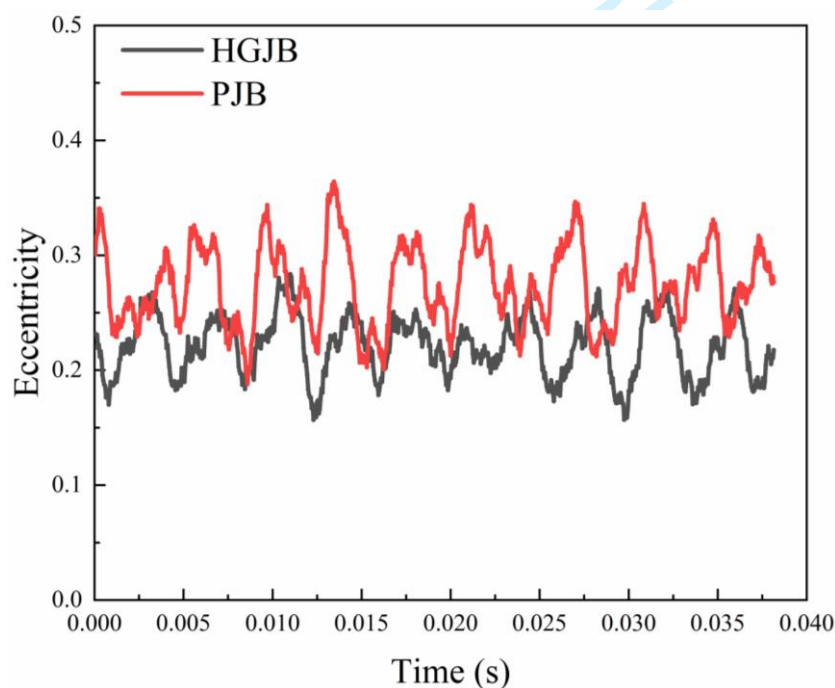


Fig. 12 Eccentricities of the HGJB and PJB vary with time.

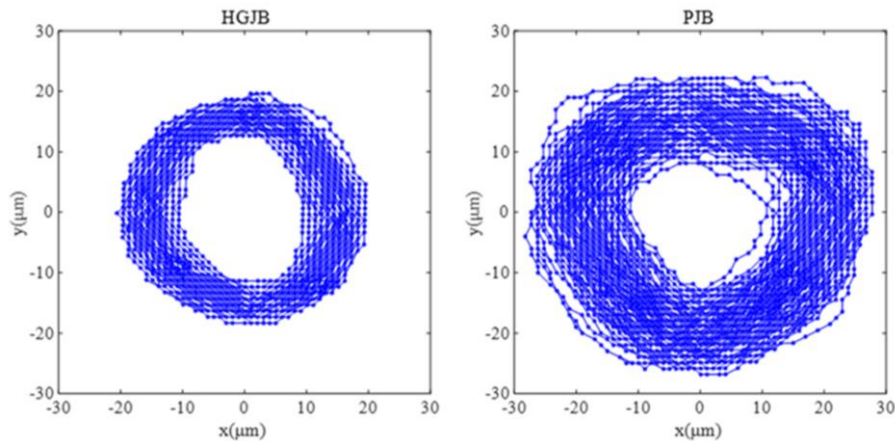


Fig. 13 Whirl trajectories of the HGJB and PJB within 0.5 s.

5. Conclusion

In this work, we developed a HGJB for the hydraulic suspension micro-pump. The CFD simulation and rotor dynamics calculation were combined to compare the dynamic and static characteristics of the HGJB and PJB. The results show that the HGJB has better working performance in a specific range of eccentricities, which can be explained by the pumping effect caused by the herringbone groove. Furthermore, the rotor dynamics calculation shows that the HGJB has better operational stability than the PJB when the eccentricity is less than 0.4 and greater than 0.62. We fabricated a prototype of the HGJB and established a set of laser displacement testing facilities to observe the trajectory of the journal in the HGJB and PJB. According to the experimental results, the operational stability of the HGJB is stronger than that of the PJB at the typical working speed of the micro-pump. The whirl range of the journal decreases by 29.61% in the X direction and by 24.09% in the Y direction. Therefore, it can be concluded that the herringbone grooved structure can significantly suppress the whirl of the journal, reducing the risk of contact wear. HGJBs have a positive effect on improving the operational stability of hydraulic suspension micro-pump.

Acknowledgments

This work was supported by the Open Fund of Science and Technology on Thermal Energy and Power Laboratory (No. TPL 2019B03).

References:

- [1] Nisar A, Afzulpurkar N, Mahaisavariya B. MEMS-based Micro-Pumps in Drug Delivery and Biomedical Applications. *Sensors Actuat B-Chem*, 2008, 130: 917-942
- [2] Tsai N C, Sue C Y. Review of MEMS-based Drug Delivery and Dosing Systems. *Sensor Actuat A-Phys*, 2007, 2: 555-564
- [3] Morshuis M, El-Banayosy A, Arusoglu L et al. European Experience of DuraHeart (TM) Magnetically Levitated Centrifugal Left Ventricular Assist System. *Eur J Cardio-Thorac*, 2009, 6: 1020-1028
- [4] Morshuis M, Schoenbrodt M, Nojiri C et al. DuraHeart (TM) Magnetically Levitated Centrifugal Left Ventricular Assist System for Advanced Heart Failure Patients. *Expert Rev Med Devic*, 2010, 2: 173-183
- [5] Luo X B, Hu R, Liu S et al. Heat and Fluid Flow in High-Power LED Packaging and Applications. *Prog Energ Combust*, 2016, 1-32
- [6] Wu R K, Fan Y W, Hong T et al. An Immersed Jet Array Impingement Cooling Device with Distributed Returns for Direct Body Liquid Cooling of High Power Electronics. *Appl Therm Eng*, 2019, 162, 114259
- [7] Liu P, Ren T, Ge Y et al. Performance Analyses of a Novel Finned Parabolic Trough Receiver with Inner Tube for Solar Cascade Heat Collection. *Sci China Tech Sci*, 2023, 5: 1417-1434
- [8] Zhang J, Chen Y, Liu Y et al. Experimental Investigation on Heat Transfer Characteristics of Microcapsule Phase Change Material Suspension in Array Jet Impingement. *Sci China Tech Sci*, 2022, 7: 1634-1645
- [9] Mohith S, Karanth P N, Kulkarni S M. Recent Trends in Mechanical Micropumps and Their Applications: A Review. *Mechatronics*, 2019, 34-55
- [10] Li H Y, Liu J K, Li K et al. A Review of Recent Studies on Piezoelectric Pumps and Their Applications. *Mech Syst Signal Pr*, 2021, 151:107393
- [11] Wang X Y, Cheng C, Wang S L et al. Electroosmotic Pumps and their Applications in Microfluidic Systems. *Microfluid Nanofluid*, 2009, 2: 145-162
- [12] Johnson M J, Go D B. Recent Advances in Electrohydrodynamic Pumps Operated by Ionic Winds: A Review. *Plasma Sources Sci T*, 2017, 26: 103002
- [13] Yang H, Jia H, Zhu Z C et al. Review of the Hydraulic and Structural Design of High-Speed Centrifugal Pumps. *Front Energy Res*, 2022,10
- [14] Wang C, Wang F, An D et al. A General Alternate Loading Technique and its Applications in the Inverse Designs of Centrifugal and Mixed-Flow Pump Impellers. *Sci China Tech Sci*, 2021, 4: 898-918
- [15] Yamane T. The Present and Future State of Nonpulsatile Artificial Heart Technology. *J Artif Organs*, 2002, 5: 149-155
- [16] Pagani F D. Continuous-Flow Rotary Left Ventricular Assist Devices with "3Rd Generation" Design. *Semin Thorac Cardio*, 2008, 3: 255-263
- [17] Kink T, Reul H. Concept for a New Hydrodynamic Blood Bearing for Miniature Blood Pumps. *Artif Organs*, 2004, 10: 916-920
- [18] Wu R K, Duan B, Liu F L et al. Design of a Hydro-Dynamically Levitated Centrifugal Micro-Pump to the Active Liquid Cooling System. 18th International Conference on Electronic Packaging Technology (ICEPT): 2017. 402-406

- 1
2
3 [19] Luo X B, Liu F L, Duan B et al. Micro Hydraulic Suspension Mechanical Pump. US patent:
4 10495093B2, 2017
5
6 [20] Kumar S, Kumar V, Singh A K. Influence of Lubricants on the Performance of Journal Bearings -
7 a Review. Tribol-Mater Surf In, 2020, 2: 67-78
8
9 [21] Garg H C, Sharda H B, Kumar V. On the Design and Development of Hybrid Journal Bearings: A
10 Review. Tribotest, 2006, 12: 1-19
11
12 [22] Tian L, Wang W J, Peng Z J. Nonlinear Effects of Unbalance in the Rotor-Floating Ring Bearing
13 System of Turbochargers. Mech Syst Signal Pr, 2013, 1-2: 298-320
14
15 [23] Chen S K, Chou H C, Kang Y. Stability Analysis of Hydrodynamic Bearing with Herringbone
16 Grooved Sleeve. Tribol Int, 2012, 15-28
17
18 [24] Gad A M, Nemat-Alla M M, Khalil A A et al. On the Optimum Groove Geometry for Herringbone
19 Grooved Journal Bearings. J Tribol-T ASME, 2006, 3: 585-593
20
21 [25] Ku R. Dynamic Characteristics of Hard Disk Drive Spindle Motors – Comparison Between Ball
22 Bearings and Hydrodynamic Bearings. J Tribol-T ASME, 1996, 118: 402-406
23
24 [26] Zhu J, Ono K. A Comparison Study on the Performance of Four Types of Oil Lubricated
25 Hydrodynamic Thrust Bearings for Hard Disk Spindles. J Tribol-T ASME, 1999, 121: 114-120
26
27 [27] Xu J, Jiao C, Zou D et al. Study on the Dynamic Behavior of Herringbone Gear Structure of Marine
28 Propulsion System Powered by Double-Cylinder Turbines. Sci China Tech Sci, 2022, 3: 611-630
29
30 [28] Hirayama T, Yamaguchi N, Sakai S et al. Optimization of Groove Dimensions in Herringbone-
31 Grooved Journal Bearings for Improved Repeatable Run-Out Characteristics. Tribol Int, 2009, 5:
32 675-681
33
34 [29] Muijderman E A. Spiral Groove Bearings. Ind Lubr Tribol, 1965, 17: 12-17
35
36 [30] Chen S K, Chou H C, Kang Y. Stability Analysis of Hydrodynamic Bearing with Herringbone
37 Grooved Sleeve. Tribol Int, 2012, 15-28
38
39 [31] Sahu M, Sarangi M, Majumdar B C. Thermo-Hydrodynamic Analysis of Herringbone Grooved
40 Journal Bearings. Tribol Int, 2006, 11: 1395-1404
41
42 [32] Han Y, Xiong S, Wang J. A New Singularity Treat-Ment Approach for Journal-Bearing Mixed
43 Lubrication Modeled by the Finite Difference Method with a Herring-Bone Mesh. J Ttribol-T
44 ASME, 2016, 138 (1): 011704
45
46 [33] Zirkelback N, San Andres L. Finite Element Analysis of Herringbone Groove Journal Bearings: A
47 Parametric Study. J Tribol-T ASME, 1998, 2: 234-240
48
49 [34] Jang G H, Yoon J W. Nonlinear Dynamic Analysis of a Hydrodynamic Journal Bearing Considering
50 the Effect of a Rotating or Stationary Herringbone Groove. J Tribol-T ASME, 2002, 2: 297-304
51
52 [35] Hirs G G. The Load Capacity and Stability Characteristics of Hydrodynamic Grooved Journal
53 Bearings. ASLE Trans, 1965, 8: 296-305
54
55 [36] Gao S Y, Shi Y G, Xu L S et al. Investigation on Influences of Herringbone Grooves for the
56 Aerostatic Journal Bearings Applied to Ultra-High-Speed Spindles. P I Mech Eng C-J Mec, 2019,
57 16: 5795-5812
58
59 [37] Ikeda S, Arakawa Y, Hishida N et al. Herringbone-Grooved Bearing with Non-Uniform Grooves
60 for High-Speed Spindle. Lubr Sci, 2010, 9: 377-392
[38] Xing G Y, Xue S, Hong T et al. A Novel Hydrodynamic Suspension Micropump Using Centrifugal
Pressurization and the Wedge Effect. Sci China Tech Sci, 2023, (in pressed)
[39] Wang Bin, Sun Y T, Ding Q. Dynamic Characteristics of the Herringbone Groove Gas Journal
Bearings: Numerical Simulations. Shock Vib, 2016, 2016: 1-13

- 1
2
3 [40] Ingram T G. Stability of a Viscous Liquid Contained Between Two Rotating Cylinders. In, ed.
4 Philosophical Transactions of the Royal Society of London. London: 1923. 289-343
5
6 [41] Gao G, Yin Z, Jiang D et al. Numerical Analysis of Plain Journal Bearing under Hydrodynamic
7 Lubrication by Water. Tribol Int, 2014, 31-38
8
9 [42] Rowe W B, Chong F S. Computation of Dynamic Force Coefficients for Hybrid
10 (Hydrostatic/Hydrodynamic) Journal Bearings by the Finite Disturbance and Perturbation
11 Techniques. Tribol Int, 1986, 19: 260-271
12
13
14
15
16
17
18
19
20
21
22
23
24
25
26
27
28
29
30
31
32
33
34
35
36
37
38
39
40
41
42
43
44
45
46
47
48
49
50
51
52
53
54
55
56
57
58
59
60

For Review Only